THE GEOLOGICAL SOCIETY OF AMERICA®

The long-lived transcrustal magmatic systems of Southeast China in response to paleo-Pacific plate subduction, recorded by the Cretaceous volcanic sequences in southeastern Zhejiang Province

Liang Liu[1], Jie-Hua Yang[1,†], Li-Fang Kang[1,2], Hong Zhong[1], and Xing-Chun Zhang[1]
[1]*State Key Laboratory of Ore Deposit Geochemistry, Institute of Geochemistry, Chinese Academy of Sciences, Guiyang 550081, China*
[2]*College of Earth Sciences, University of Chinese Academy of Sciences, Beijing 100049, China*

ABSTRACT

Processes taking place in subduction zones are highly debated. The Cretaceous volcanic rocks are voluminously distributed along the coastal area of southeastern (SE) China. To elucidate their petrogenesis and relationship with subduction, we use new zircon U-Pb ages and Hf-O isotopes for the representative Cretaceous volcanic sequences in Zhejiang Province, China. According to stratigraphic investigations, zircon U-Pb ages, and Hf-O isotopes, these volcanic rocks can be divided into different groups corresponding to three stages of volcanic activity: the early (Stage 1, 136–129 Ma), middle (Stage 2, 125–115 Ma), and late (Stage 3, 110–94 Ma) stages. Diverse zircon populations (including antecrysts, autocrysts, and xenocrysts) are recognized. Hf-O isotopes of autocrysts suggest different protoliths for the identified three stages of volcanic activity. Xenocrysts show obvious different compositions from autocrysts. Antecrysts share similar compositions with autocrysts, which favor similarities in the magmas from which they were generated. Our observations (very small age intervals between antecrysts and autocrysts, sources for volcanic rocks throughout the entire crust, and volcanic magmatism with long-term and discontinuous characteristics), were inconsistent with the traditional melt-dominated magma chamber model. Consequently, we propose that those volcanic rocks were derived from long-lived transcrustal magmatic systems (TCMS), dominated by crystal mush, instead of melt-dominated magma chambers, maintained and recharged by a discontinuous contribution of contemporaneous underplated mantle-derived magmas, triggered by paleo-Pacific plate subduction. We suggest the different stages of volcanic activity and corresponding long-lived TCMS were produced by the change of Pacific plate motion beneath SE China during the Cretaceous period.

1. INTRODUCTION

Subduction zones serve as major places of mass and energy exchange between crust and mantle and generate voluminous magmas that record the formation and evolution of continental crust (Guo et al., 2021). Magmatism in subduction zones is generally dominated by andesites and mafic igneous rocks (Kelemen et al., 2013). These igneous rocks are generally characterized by enrichments in large-ion lithophile elements (LILEs) and light rare earth elements (LREEs) relative to high field strength elements (e.g., Nb and Ta) (Plank et al., 2013), which are widely believed to be a result of the preferential mobilization of LILEs or LREEs in fluids from the slab to mantle wedge (Spandler and Pirard, 2013). However, the late Mesozoic magmatism in southeastern (SE) China is characterized by the emplacement of voluminous felsic magmas with a few andesites and mafic magmas, which are considered to have been resulted from the subduction of the paleo-Pacific Ocean (Li et al., 2019; Li and Li, 2007; Xu et al., 2021; Zhou et al., 2006). Although these igneous rocks have been studied in terms of petrogenesis, tectonic settings, and geodynamics, the key factors for controlling magma compositions, are still not clear (Chen et al., 2008, 2016). Recently, Guo et al. (2021) proposed that a tectonic transition in the Cretaceous from advanced subduction to rollback-tearing of the paleo-Pacific slab was a response to the emplacement of both the arc-type and ocean island basalt-like mafic magmatism in SE China. However, the possible factors, such as source compositions, fractional crystallization, crustal contamination, magma mixing, or tectonic regime, may affect the chemical compositions of those felsic igneous rocks (Liu et al., 2016; Wu et al., 2017), which need to be further evaluated and clarified.

Meanwhile, the relationship between magmatism and slab subduction also remains controversial (He and Xu, 2012; Li and Li, 2007; Sun et al., 2007; Xu et al., 2021; Zhou et al., 2006). Many tectonic models related to paleo-Pacific plate subduction have been postulated to explain the late Mesozoic tectono-magmatic evolution of SE China (Chen et al., 2008; Gilder et al., 1991; Hsü et al., 1990; Li, 2000; Li and Li, 2007; Sun et al., 2007; Zhou et al., 2006). For example, Zhou and Li (2000) suggested that the dip angle of subducted paleo-Pacific slab increased progressively during the period from 180 to 80 Ma. During this period, mantle wedge melting and basaltic underplating provided the necessary heat to trigger partial melting of the continental crust. Alternatively, Li and Li (2007) presented a flat-slab subduction and slab-foundering model to account for the broad Mesozoic intracontinental deformation and magmatism within South China. In particular, many models have been paid much attention to the Cretaceous period. He and Xu (2012) raised that subduction of the paleo-Pacific plate beneath SE China evolved from slab advance to slab rollback at ca. 110 Ma. While Li et al. (2014d) speculated the existence of break-off (at ca. 125–115 Ma) and rollback (at ca. 115–90 Ma) of the subducting Paleo-Pacific Plate during the Cretaceous. Based on geological, geochronological, and geochemical data of the Cretaceous volcanic sequences in the Zhejiang-Fujian provinces, Liu et al. (2016) proposed a not synchronized paleo-Pacific slab rollback model to account for the spatial-temporal migration of late Mesozoic igneous rocks in SE China. Importantly, different directions of subduction motion for the paleo-Pacific plate in the Cretaceous were proposed. These include suggestions that the slab drifted northwestward (Li et al., 2014a, 2014b; Li and Li, 2007; Liu

†Corresponding author: yangjiehua@vip.gyig.ac.cn.

GSA Bulletin; May/June 2023; v. 135; no. 5/6; p. 1091–1108; https://doi.org/10.1130/B36448.1; 12 figures; 1 supplemental file.
published online 3 August 2022

et al., 2016; Zhou and Li, 2000; Wang et al., 2017), northeastward followed by northwestward (changed at ca. 140 Ma; Liu et al., 2012b), or southwestward followed by northwestward (changed at ca. 125 Ma; Liu et al., 2018; Sun et al., 2007; Wang et al., 2011a).

Cretaceous volcanisms are widespread along the coastal area of SE China (Fig. 1) (Chen et al., 2008; Chen et al., 2016; Liu et al., 2014b, 2012a, 2016), which received less attention than the coeval granites (Guo et al., 2012; Meng et al., 2012; Zhou et al., 2006). The Cretaceous volcanic rocks are dominated by rhyolites as both pyroclastic rocks and lava flows with a total thickness of more than 5 km, while andesitic and mafic rocks are less than 5 vol% (Xu et al., 2021). The Cretaceous felsic volcanic successions in SE China are best developed in Zhejiang Province (Fig. 1) ranging from 140 to 88 Ma (Liu et al., 2012a). Studies on these Cretaceous volcanic rocks are of great significance since they can provide important signatures for the dominant mechanism controlling chemical compositions of continental arc magmatism, and magma storage, accumulation, and chemical differentiation in the continental crust (Xu et al., 2021), and may help us to better understand how long-lived magmatic systems relate to the periodicity of large volcanic eruptions (Liu and Lee, 2020).

Our study focuses on these Cretaceous volcanic rocks in SE Zhejiang Province. Zircon has long been recognized as the most resistant mineral and the key geochemical tracer in terms of U-Pb age and Hf-O isotopes in felsic magmas (Kemp et al., 2007; Miller et al., 2007). More importantly, O-isotopic systematics is sensitive to crust-mantle interaction in subduction zones, because different sources for the origin of arcs have distinctly different O-isotope compositions (Zhao et al., 2019). Detailed zircon U-Pb dating of the entire volcanic sequences defines the

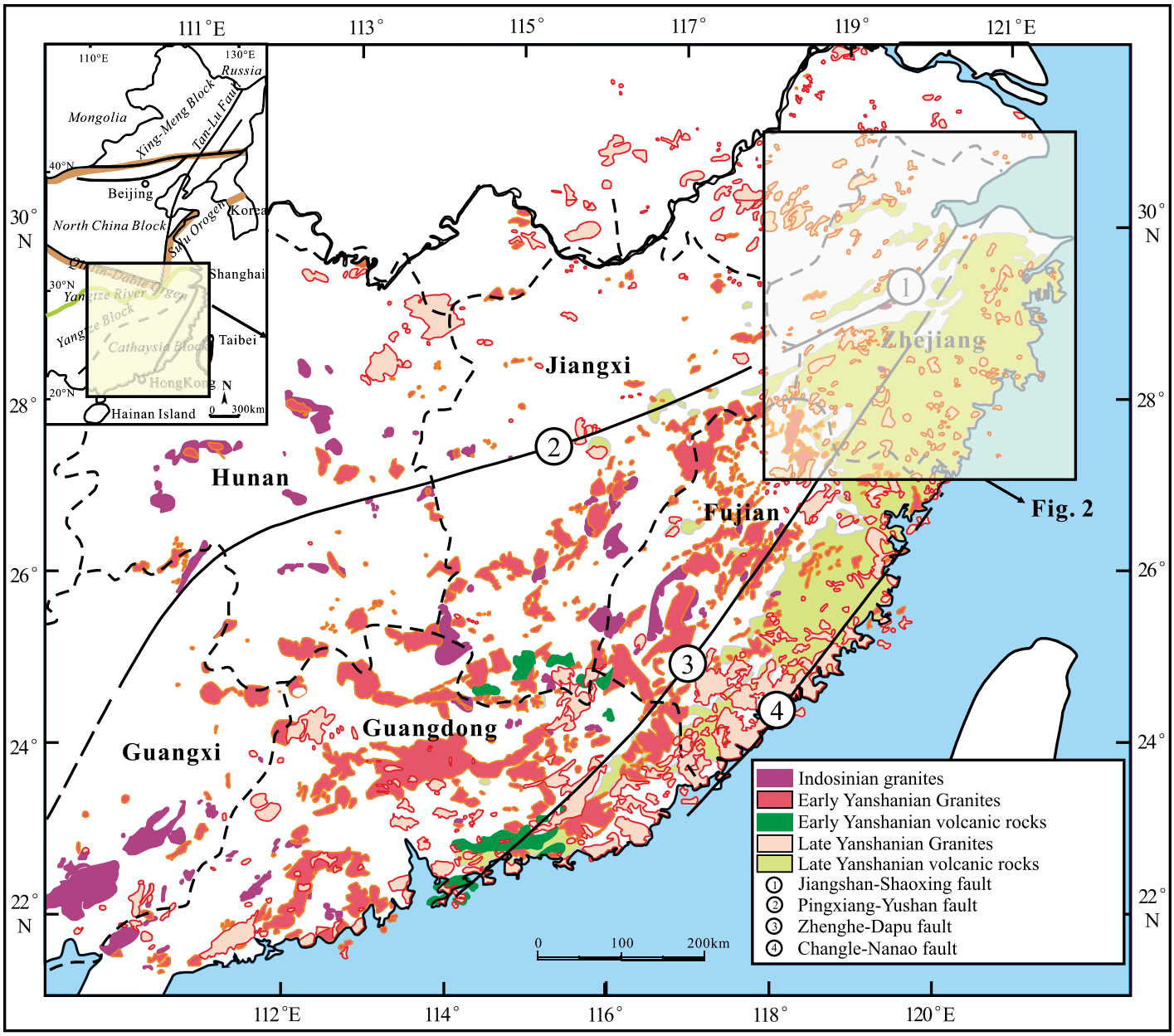

Figure 1. Simplified geological map of south China showing the distribution of Mesozoic granitoid and volcanic rocks. Modified after Zhou et al. (2006).

geochronological framework of the Cretaceous magmatism, and related systematical zircon Hf-O isotope analysis elucidates the nature of the source region for magmas of subduction zone volcanic rocks. Our new data combined with previous studies could be useful not only for examining the fundamental magmatic processes of the Earth's crust but also for a better understanding of the relationship between magmatism and subduction.

2. GEOLOGICAL SETTING

South China Block (SCB) is one of the major igneous provinces of the world, and its Mesozoic magmatism is an important part of the circum-Pacific magmatic belt (Xu et al., 2021). It consists of the Yangtze Block to the west and the Cathaysia Block to the east which were welted together along the Jiangnan Fold Belt during the Neoproterozoic (Fig. 1) (Zhao and Cawood, 2012; Zhao et al., 2011). The Cathaysia Block has been considered as a composite unit comprising several discrete continental blocks (Xu et al., 2007; Yu et al., 2010), which mainly consists of Neoproterozoic to Phanerozoic sedimentary rocks and Paleozoic to Mesozoic igneous rocks with minor pre-Neoproterozoic basement rocks (Li et al., 2014c; Yu et al., 2010; Zheng et al., 2011). The Precambrian basement rocks are sparsely exposed in the Chencai, Badu, Wuyishan, Nanling, Yunkai, and Hainan areas in a NE-trending belt delimited by the Chenzhou-Linwu–Jiang-Shao Fault to the northwest and the Zhenghe-Dapu Fault to the southeast (Zhao and Cawood, 2012).

The Paleozoic and Mesozoic magmatism in SCB has been classified into the Caledonian (early–middle Paleozoic), Indosinian (Triassic), Early Yanshanian (Jurassic), and Late Yanshanian (Cretaceous) magmato-tectonic events (Li and Li, 2007; Xing et al., 2004; Zhou et al., 2006). An abundance of igneous rocks, especially granites, formed in response to these events, with the granites in the easter SCB commonly regarded as a large granite province (Wang and Zhou, 2005). Late Mesozoic magmatism was largely concentrated in the Cathaysia Block, and the intensity of magmatism increased toward the ocean (Fig. 1) (Zhou et al., 2006). Associated granitoids with Jurassic ages are concentrated in the inland region, whereas those with Cretaceous ages are mainly distributed in the coastal region. Volcanic rocks were erupted mainly in the Cretaceous and generally crop out along the coastal area of SE China (Zhou et al., 2006); they were traditionally divided into the lower and upper volcanic series that are separated by a ubiquitous regional unconformity (He and Xu, 2012; Lapierre et al., 1997; Liu et al., 2012a). The lower volcanic series (140–110 Ma) consists mainly of rhyolitic and dacitic rocks with sporadic andesite and basalt, whereas the upper volcanic series (110–85 Ma) comprises predominant rhyolite and minor basalt (Fig. 2) (Chen et al., 2008; He and Xu, 2012; Lapierre et al., 1997; Liu et al., 2012a).

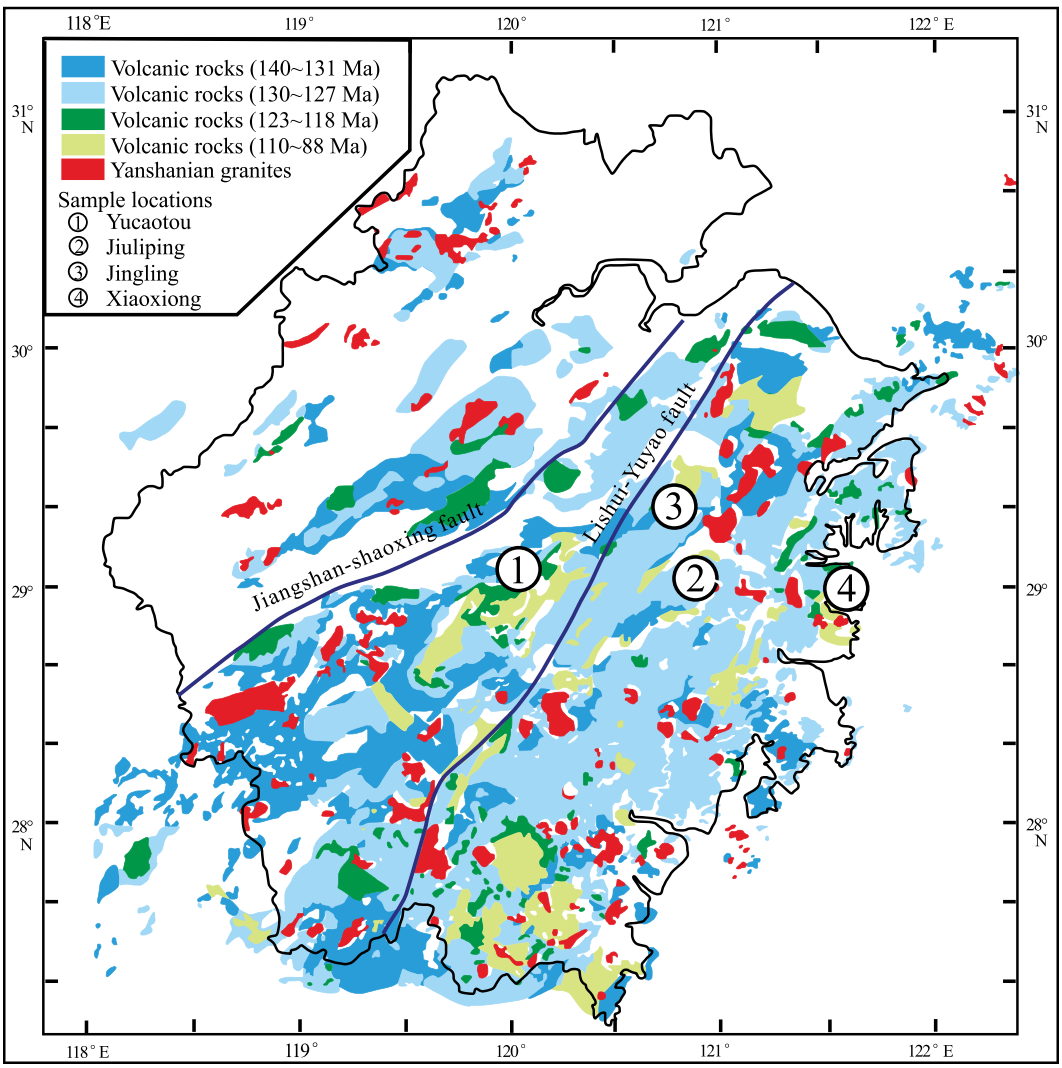

Figure 2. Distribution of Cretaceous volcanic rocks in Zhejiang Province, China, and sample locations. Modified after Liu et al. (2014b).

3. VOLCANIC SEQUENCES AND SAMPLE DESCRIPTIONS

The Early Cretaceous volcanic rocks (the lower volcanic series) from the southeastern Zhejiang Province are named the Moshishan Group, which consist of the Dashuang, Gaowu, Xishantou, Chawan, Jiuliping formations (Fig. 3A) (Liu et al., 2014b, 2012a). According to the Yucaotou stratigraphic section in Yiwu City, Jiuliping stratigraphic section in Tiantai City, and Xiaoxiong Section in Sanmen City (Figs. 3B–3D), the Dashuang Formation mainly contains rhyolitic ignimbrite and tuff with minor tuffaceous sandstone and mudstone; the Gaowu Formation consists of rhyolitic ignimbrite and tuff; the Xishantou Formation is composed of sandstone and rhyolitic tuff, vitro-crystalline tuff and ignimbrite, silicified sedimentary tuff, and rhyolitic ignimbrite and tuff; the Chawan Formation contains rhyolitic breccia-bearing vitric tuff and rhyolitic ignimbrite; the Jiuliping Formation is composed of mudstone and sandstone, sedimentary tuff and

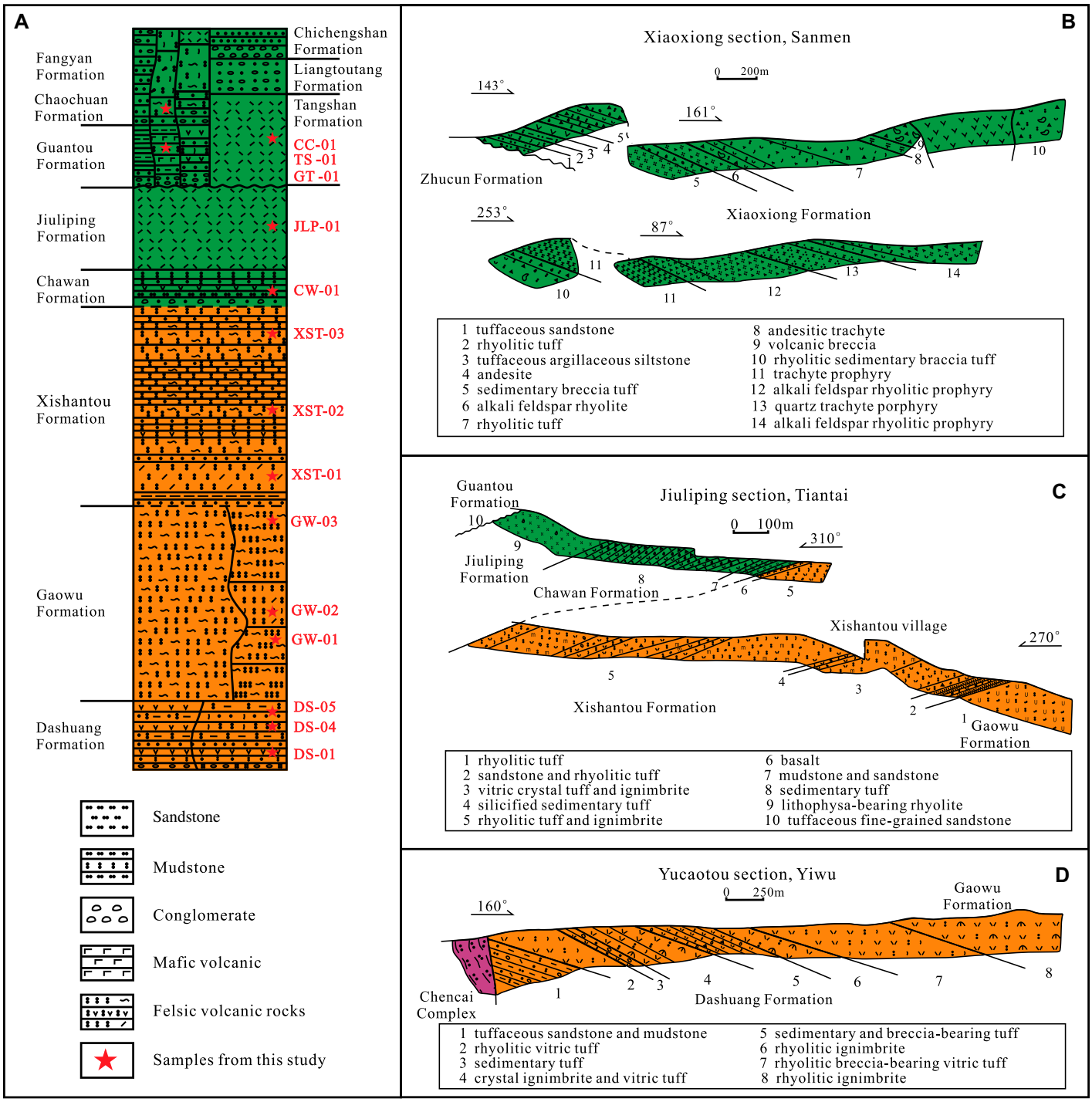

Figure 3. Columnar section and profiles of representative sections from where the studied samples were collected in Zhejiang Province, China. Modified from Liu et al. (2012a), Wong and Yu (1999), and Zhang et al. (2018).

lithophysa-bearing rhyolite. Three samples (DS-01, DS-04, and DS-05) collected from the Dashuang Formation are breccia-bearing lithic tuff, crystal tuff, and litho-crystalline tuff, respectively (Fig. 4A). Four samples (GW-01, GW-02, GW-03, and GW-04) from the Gaowu Formation were all litho-crystalline ignimbrite (Fig. 4B). Three samples (XST-01, XST-02, and XST-03) from the Xishantou Formation are crystal-vitroclastic ignimbrite (Fig. 4C). One sample (CW-01) from Chawan Formation is sedimentary tuff (Fig. 4D). One sample (JLP-01) from Jiuliping Formation is rhyolite (Fig. 4E).

The Late Cretaceous volcanic rocks (the upper volcanic series) are only preserved in some small basins of southeastern Zhejiang Province, represented by the Yongkang Group, the Tiantai Group, and the Xiaoxiong Formation. The Yongkang Group comprises the Guantou, Chaochuan, and Fangyan formations. The Tiantai Group includes the Tangshang, Liangtoutang, and Chichengshan formations. The Guantou Formation consists of tuffaceous fine-grained sandstone, ignimbrite, and lava flow. The Chaochuan Formation comprises litho-crystalline tuff. The Xiaoxiong Formation could be divided into two segments (Fig. 3): the lower segment is made up of rhyolitic tuff, alkali-feldspar rhyolite, and sedimentary tuff, with sandstone and siltstone at the bottom; while the upper segment consists of rhyolitic tuff, alkali-feldspar rhyolite, and trachyte. Central intrusive porphyritic syenite exposes in the caldera (Liu et al., 2012a). One sample (GT-01) from the Guantou Formation is ignimbrite (Fig. 4F). One sample (CC-01) from the Chaochuan Formation is litho-crystalline tuff (Fig. 4G). One sample (TS-01) from Tangshang Formation is litho-crystalline tuff (Fig. 4H). One sample (XX-01) from the Xiaoxiong Formation is tuff (Fig. 4I).

4. ANALYTICAL METHODS

Fifteen samples were selected for whole major and trace element analyses; the representative zircon grains were selected for

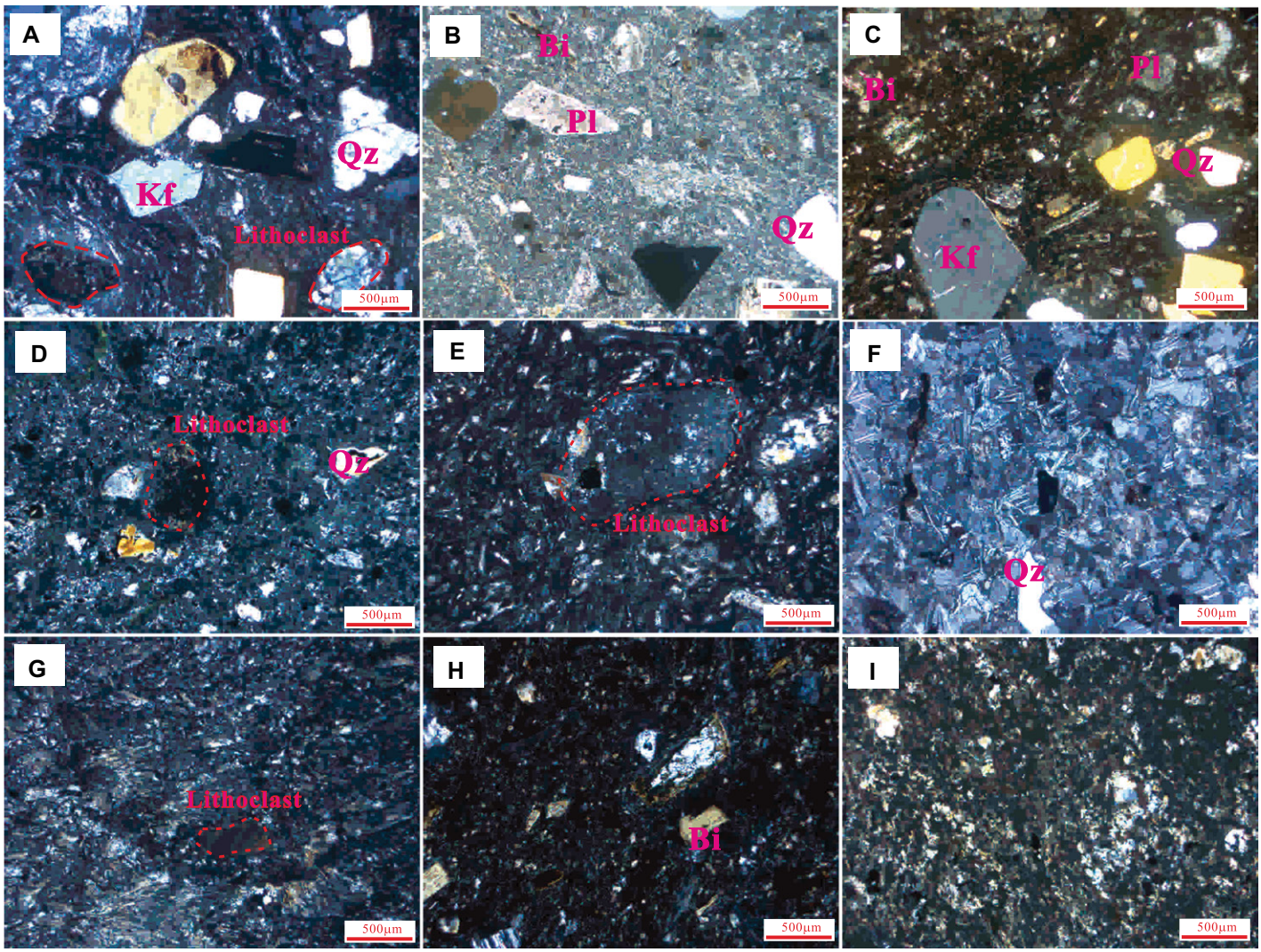

Figure 4. Photomicrographs of representative volcanic rocks from southeastern Zhejiang Province, China (crossed nicols). (A) Litho-crystalline tuff from the upper part of the Dashuang Formation; (B) lithic crystal ignimbrite from the upper part of the Gaowu Formation; (C) crystal ignimbrite from the lower part of the Xishantou Formation; (D) sedimentary tuff from the lower part of the Chawan Formation; (E) lithophysa rhyolite from the upper part of the Jiuliping Formation; (F) ignimbrite from the lower part of the Guantou Formation; (G) litho-crystalline tuff from the lower part of the Chaochuan Formation; (H) litho-crystalline tuff from the upper part of the Tangshang Formation; (I) tuff from the upper part of the Xiaoxiong Formation. Mineral abbreviations: Qz—quartz; Kf—K-feldspar; Pl—plagioclase; Bi—biotite.

cathodoluminescence (CL) imaging, U-Pb dating, trace element, and Hf-O isotopic studies.

4.1. Whole-Rock Major and Trace Elements

Rock samples were cut into small pieces and fresh parts were selected and ground into powder for whole-rock geochemical analyses. Both the whole-rock major and trace elements were analyzed at the State Key Laboratory of Ore Deposit Geochemistry (SKLODG), Institute of Geochemistry, Chinese Academy of Sciences (IGCAS), Guiyang, China. Major elements were analyzed using a Thermo Fisher ARL Perform'X 4200 X-ray fluorescence spectrometer. Loss-on-ignition values were measured by heating 1 g sample powder to 1000 °C for 1 h.

Trace-element analyses were conducted using a Plasma Quant-MS Elite inductively coupled plasma–mass spectrometer (ICP-MS). For each analysis, a 50 mg subsample of rock powder was dissolved at 190 °C in a mixture of HF (1 mL) and HNO_3 (1 mL), and placed in a PTFE-lined (polytetra-fluoroethylene) stainless-steel bomb for 48 h. To monitor signal drift during counting, Rh was applied as an internal standard. International standards GBPG-1, AGV-2, and AMH-1 were used to monitor analytical quality, with analytical accuracy generally better than ±10%. Details of the experimental procedures followed are given by Qi et al. (2000).

4.2. U-Pb Dating and Trace Element Analyses of Zircon by Laser Ablation (LA)-ICP-MS

U-Pb dating and trace element analyses of zircon were conducted synchronously by LA-ICP-MS at SKLODG, IGCAS. Laser sampling was performed using a GeoLas Pro 193 nm ArF excimer laser. An Agilent 7900 ICP-MS instrument was used to acquire ion-signal intensities. Helium was applied as a carrier gas which was mixed with Argon via a T-connector before entering the ICP-MS. Each analysis incorporated a background acquisition of ~18 s (gas blank) followed by 50 s of data acquisition from the sample. During analysis, the laser beam diameter, repetition rate, and energy density were 32 μm, 5 Hz, and 5.0 J/cm^2, respectively. Off-line selection and integration of background and analyte signals, as well as time-drift correction and quantitative calibration for trace element analyses and U-Pb dating, were performed by ICPMSDataCal software (Liu et al., 2010). Zircon 91500 was used as an external standard for U-Pb dating and was analyzed twice every 6–8 analyses (i.e., 2 zircon 91500 + 6–8 samples + 2 zircon 91500). Uncertainty of preferred values for the external standard 91500 was propagated to the ultimate results of the samples. Concordia diagrams and weighted mean calculations were made using Isoplot software (Ludwig, 2008). Trace element compositions of zircons were calibrated against multiple-reference materials (NIST 610, BHVO-2G, BCR-2G, and BIR-1G) combined with Zr internal standardization. The preferred values of element concentrations for the U.S. Geological Survey reference glasses are from the GeoReM database (http://georem.mpch-mainz.gwdg.de/).

4.3. Zircon LA-Multicollector (MC)-ICP-MS Lu-Hf Isotope

Hafnium isotopic ratios of zircon were conducted by LA-MC-ICP-MS at SKLODG, IGCAS. Australian Scientific Instruments RESOlution-LR laser ablation system and Nu Instruments Nu Plasma III MC-ICP-MS (Wrexham, Wales, UK) were combined for the experiments. The 193 nm ArF excimer laser, homogenized by a set of beam delivery systems, was focused on the zircon surface with a fluence of 6.0 J/cm^2. The ablation protocol employed a spot diameter of 40 μm at a 6 Hz repetition rate for 40 s (equating to 240 pulses). Helium was applied as a carrier gas to efficiently transport aerosol to MC-ICP-MS. Five standard zircons (including GJ-1, 91500, Plešovice, Mud Tank, and Penglai) were applied for quality control. Mass bias effects on Hf were corrected using an exponential law and a reliable value for $^{179}Hf/^{177}Hf$ of 0.7325. In this study, measurements of zircon standard 91500, GJ-1, Penglai, Plešovice, Mud Tank gave $^{176}Hf/^{177}Hf$ of 0.282302 ± 0.000008 ($n = 23$; 2σ), 0.282011 ± 0.000008 ($n = 23$; 2σ), 0.282907 ± 0.000003 ($n = 106$; 2σ), 0.282471 ± 0.000005 ($n = 25$; 2σ), 0.282506 ± 0.000007 ($n = 23$; 2σ), respectively, all of which are consistent with recommended values within 2σ errors (Griffin et al., 2007).

4.4. Zircon Oxygen Isotope Analyses

Zircon oxygen isotope compositions were measured before zircon U-Pb dating, using a Cameca IMS 1280-HR secondary ion mass spectrometer at the secondary ion mass spectrometry (SIMS) laboratory in the Guangzhou Institute of Geochemistry, Chinese Academy of Sciences (GIGCAS), Guangzhou, China. The detailed analytical procedures have been reported by Li et al. (2010a) and Yang et al. (2018). The Cs^+ primary ion beam was accelerated at 10 kV, with an intensity of ~2 nA (Gaussian mode with a primary beam aperture of 200 μm to reduce aberrations) and rastered over a 10 μm area. The spot is ~20 μm in diameter. The entrance slit width is ~120 μm and the exit slit width for multicollector Faraday cups (FCs) for ^{16}O and ^{18}O is 500 μm (MRP = 2500). The intensity of ^{16}O was typically 1×10^9 cps. Oxygen isotopes were measured in multicollector mode using two off-axis Faraday cups. One analysis takes ~4 min consisting of pre-sputtering (~120 s), automatic beam centering (~60 s), and integration of oxygen isotopes (10 cycles × 4 s, total 40 s). Uncertainties in individual analyses are reported at a 2σ level. With low noise on the two FC amplifiers, the internal precision of a single analysis is generally better than 0.3‰ (2σ) for the $^{18}O/^{16}O$ ratio. Values of $\delta^{18}O$ are standardized to Vienna Standard mean ocean water compositions (VSMOW) and reported in standard per mil notation. The instrumental mass fractionation factor is corrected using zircon standard 91500 with ($\delta^{18}O$) VSMOW = 9.94 ± 0.10‰ (Wiedenbeck et al., 2004). The Penglai reference zircon was used as the external standard and Qinghu reference zircon was used as unknowns for calibration. Sixty-eight measurements of the Penglai zircons during this study yield a weighted mean of $\delta^{18}O = 5.25 \pm 0.05$‰, which is identical within errors to the reported value of 5.31 ± 0.10‰ (Li et al., 2010b). Thirty-three measurements of the Qinghu zircons yield a weighted mean of $\delta^{18}O = 5.56 \pm 0.07$‰, which is also identical within errors to the reported value of 5.39 ± 0.22‰ (Li et al., 2013).

5. RESULTS

5.1. Zircon U-Pb Dating and Trace Element Compositions

A total of 15 samples from the volcanic rocks were selected for zircon U-Pb dating and trace element analysis. CL images of representative zircon grains are shown in Figure 5. Zircon U-Pb dating and trace element results are listed in Tables S1–S2[1] and are presented graphically in Figure 6. Uncertainties are quoted at 2σ for the weighted mean ages.

[1]Supplemental Material. Table S1: Zircon LA-ICP-MS U-Pb dating results of the volcanic rocks in SE Zhejiang Province. Table S2: Trace elements (ppm) in zircon from the volcanic rocks in SE Zhejiang Province acquired by LA-ICP-MS. Table S3: Major element contents (wt%) of volcanic rocks in SE Zhejiang Province. Table S4: Trace and rare earth element (ppm) analyses of volcanic rocks in SE Zhejiang Province. Table S5: Zircon in-situ Hf isotopic compositions from the volcanic rocks in SE Zhejiang Province. Table S6: Zircon in-situ O isotopic compositions from the volcanic rocks in SE Zhejiang Province. Please visit https://doi.org/10.1130/GSAB.S.20134178 to access the supplemental material, and contact editing@geosociety.org with any questions.

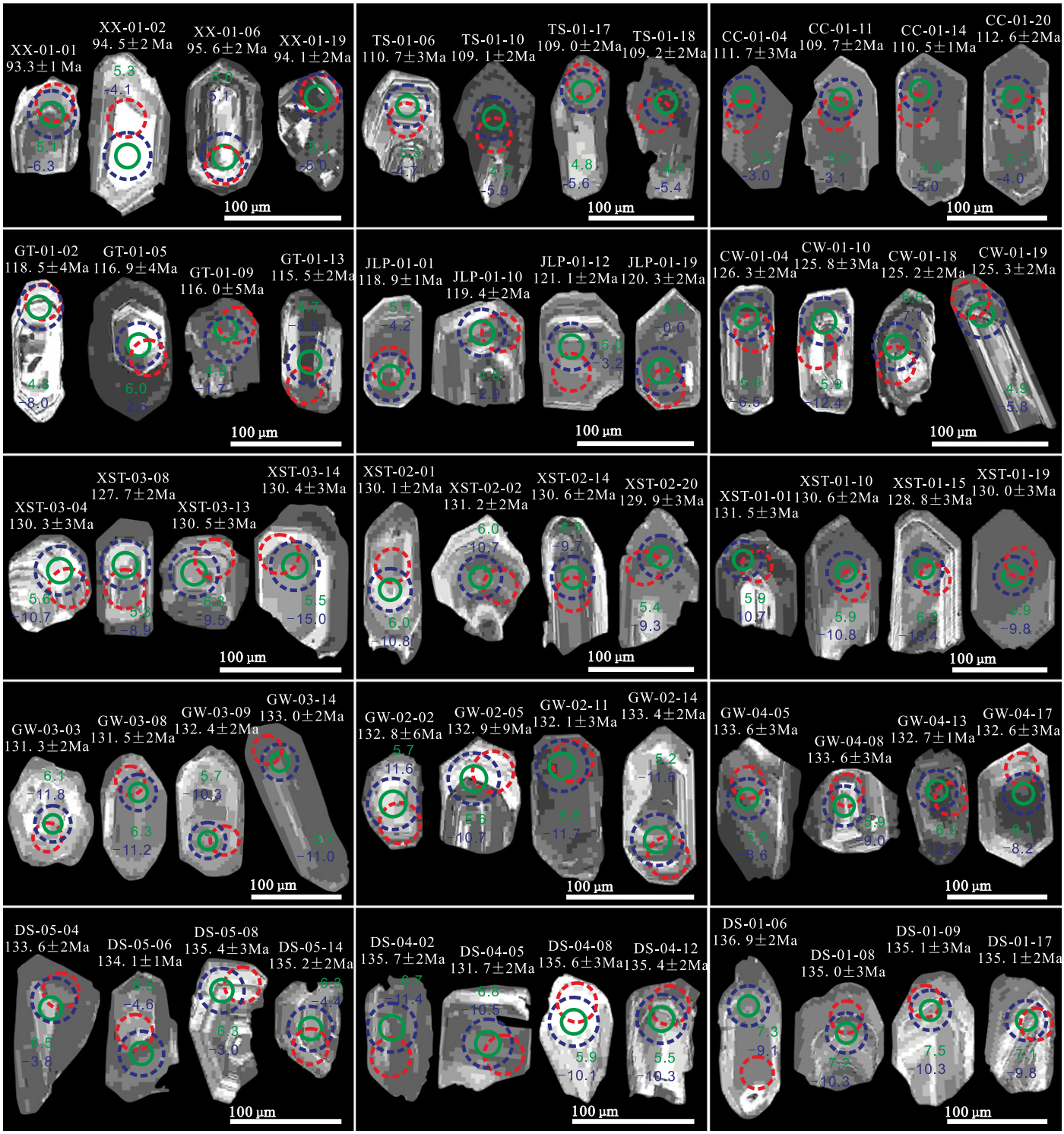

Figure 5. Representative cathodoluminescence images of selected zircons from the volcanic rocks in SE Zhejiang Province, China. The morphology of zircon grains, $^{206}Pb/^{238}U$ ages, $\varepsilon_{Hf}(t)$ values, and $\delta^{18}O$ are shown. The red circles (with dashed lines) indicate the U-Pb dating positions, large blue circles (with dashed lines) indicate the sites of Hf isotope analyses, and small green circles (with solid lines) indicate the sites of O isotope analyses. Circle diameters show the approximate laser spot sizes.

The zircon grains from the volcanic rocks are euhedral to subhedral, prismatic to elongate, and colorless to pale yellow. These grains are 70–200 μm long with length/width ratios of 1:1–2:1. They show clear oscillatory growth zonings and locally display typical zoning absorptions (Fig. 5). They have high Th/U ratios of 0.25–3.96 (Table S1), and their chondrite-normalized rare earth element (REE) patterns show signifi-

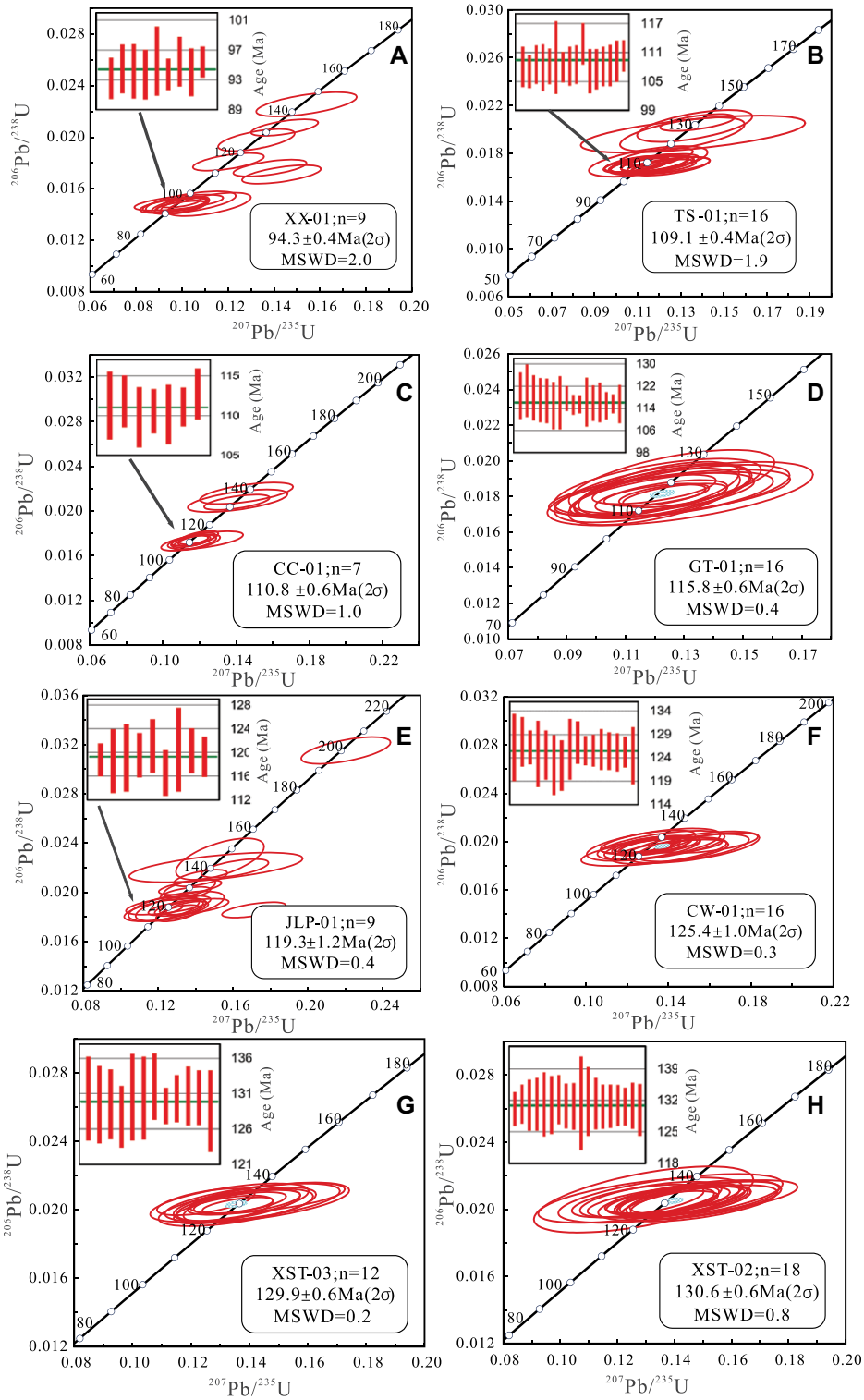

Figure 6. Laser ablation–inductively coupled plasma–mass spectrometry zircon U-Pb concordia diagrams, weighted mean $^{206}Pb/^{238}U$ ages (A–O), and chondrite-normalized rare earth element patterns (P) from the volcanic rocks in SE Zhejiang Province, China.

cant heavy REEs enrichment, positive Ce and negative Eu anomalies, consistent with an igneous origin (Fig. 6P).

If all zircon crystals crystallized from a single magma system, then the quality of geochronological data can be evaluated. However, in a multi-cyclic magmatic system, various crystal populations might be expected (Zhou et al., 2020), including xenocrysts, antecrysts, autocrysts, and inherited crystals (the terminology recommended by Miller et al., 2007). Xenocrysts correspond to those zircons incorporated from the surrounding host rocks during magma transit and emplacement. Autocrysts are zircons that grow within the youngest magma pulse, whose ages generally predate the eruption age by thousands to tens of thousands years, and could approximately represent the eruption age in view of the analytical uncertainty. Antecrysts grown within the same magma plumbing system can well share similar chemical characteristics with autocrysts as distinguished from inherited grains. In this contribution, except for those older zircons, most analyses for each formation are all concordant or nearly concordant, interpreted as autocrysts here, and plot as a cluster on the concordia curve, respectively (Fig. 6).

Except for four zircon grains that recorded older $^{206}Pb/^{238}U$ ages of 144 ± 2–116 ± 2 Ma, the other analyses from the Xiaoxiong Formation yield a weighted mean $^{206}Pb/^{238}Pb$ age of 94.3 ± 0.4 Ma (mean square weighted deviation [MSWD] = 2.0; Fig. 6A), which suggests that the eruption ended after ca. 94 Ma. Zircons from the Tangshang and Chaochuan formations give similar weighted mean $^{206}Pb/^{238}Pb$ ages of 109.1 ± 0.4 Ma (MSWD = 1.9; Fig. 6B) and 110.8 ± 1.1 Ma (MSWD = 1.0; Fig. 6C), respectively. They also record older $^{206}Pb/^{238}Pb$ ages from 131 ± 2–125 ± 4 Ma and 156 ± 2–133 ± 2 Ma, respectively.

Sixteen zircons from the Guantou Formation yield a weighted-mean $^{206}Pb/^{238}U$ age of 115.8 ± 0.6 Ma (MSWD = 0.4; Fig. 6D). One crystal from this formation records older age of 147 ± 5 Ma. Zircons from the Jiuliping and Chawan formations yield weighted mean $^{206}Pb/^{238}Pb$ ages of 119.3 ± 1.2 Ma (MSWD = 0.4; Fig. 6E) and 125.4 ± 1.0 Ma (MSWD = 0.3; Fig. 6F), respectively. Several zircons retain older ages from 200 ± 3 Ma to 127 ± 1 and 153 ± 3 Ma for both of the respective formations.

The weighted mean $^{206}Pb/^{238}Pb$ ages of 129.9 ± 0.6 Ma (MSWD = 0.2; Fig. 6G), 130.6 ± 0.6 Ma (MSWD = 0.8; Fig. 6H), and 130.8 ± 0.6 Ma (MSWD = 0.6; Fig. 6I) are obtained from the upper, middle, and lower layers of the Xishantou Formation, respectively. Three samples from the upper, middle, and lower layers of the Gaowu Formation yield weighted mean $^{206}Pb/^{238}Pb$ ages of 132.4 ± 1.2 Ma (MSWD = 0.4; Fig. 6J), 131.9 ± 0.8 Ma (MSWD = 1.0; Fig. 6K), and 132.4 ± 0.6 Ma (MSWD = 2.3; Fig. 6L),

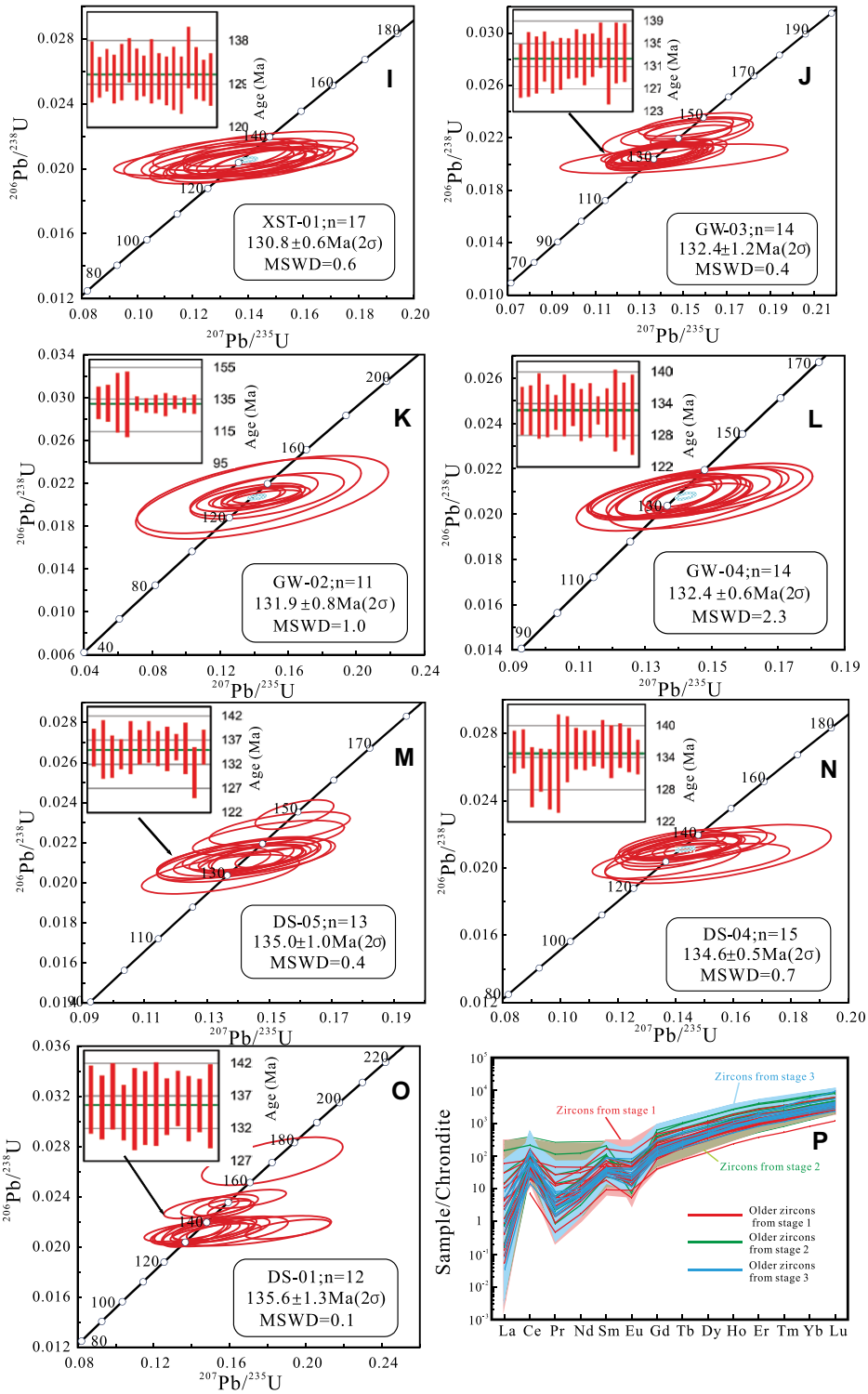

Figure 6. (*Continued*)

respectively. Zircon grains from the upper, middle, and lower layers of the Dashuang Formation give weighted mean $^{206}Pb/^{238}Pb$ ages of 134.6 ± 0.5 Ma (MSWD = 0.7; Fig. 6M), 134.6 ± 0.5 Ma (MSWD = 0.7; Fig. 6N), and 135.6 ± 1.3 Ma (MSWD = 0.1; Fig. 6O), respectively. These ages define the formation age of 136–129 Ma for these formations. Old zircons also record ages from 155 ± 4 to 152 ± 4 Ma, 147 ± 2 to 139 ± 8 Ma, and 171 ± 5 to 142 ± 2 Ma for the three formations, respectively.

5.2. Whole-Rock Major and Trace Element Characterization

Representative samples were analyzed for whole-rock major and trace element compositions that are given in Tables S3 and S4 (see footnote 1). Most samples have high SiO_2 contents varying from 72 to 81 wt% except sample XST-02 which has SiO_2 = 65 wt%. They have moderate alkali contents ($K_2O + Na_2O$ = 4.9–8.9 wt%), and thus fall into the field of rhyolite and subalkaline series on the total alkali versus silica diagram (Fig. 7). They also have low MgO (0.09–0.94 wt%), CaO (0.06–2.50 wt%), $Fe_2O_3^T$ (0.75–3.47 wt%), and TiO_2 (0.07–0.56 wt%). Whole-rock aluminum saturation indices were calculated from A/CNK = Al_2O_3/($CaO + Na_2O + K_2O$) (in molar quantities). All the volcanic rock samples have high Al_2O_3 (10.20–16.37 wt%) and A/CNK values (0.97–1.35).

The samples show similar chondrite-normalized REE patterns with fractionated LREE and flat HREE (Fig. 8A) and variable negative Eu anomalies (Eu/Eu* = 0.04–0.86). They are generally enriched in Rb, Th, and Pb, and depleted in Ba, Ta, Nb, Sr, P, and Ti in the spidergrams (Fig. 8B), similar to the typical characteristics of the continental crust (Rudnick and Gao, 2003).

5.3. Zircon Hf-O Isotopic Compositions

In situ Zircon Hf-O isotopic data are listed in Tables S5 and S6 (see footnote 1), and shown in Figures 9 and 10. The $\varepsilon_{Hf}(t)$ values and two-stage Hf model ages [T_{DM2}(Hf)] are calculated using in situ zircon U-Pb ages. For calculating the T_{DM2}(Hf) values, we assume the parental magma to have been derived from an average continental crust, with $^{176}Lu/^{177}Hf$ = 0.015, that originated from the depleted mantle source (Griffin et al., 2002). Previous studies reveal that the Cretaceous volcanism in SE China took place at multiple stages (Liu et al., 2016). These Cretaceous volcanic rocks were also traditionally divided into the lower and upper volcanic series that are separated by a ubiquitous regional unconformity at ca. 110 Ma (He and Xu, 2012; Lapierre et al., 1997). Combined with our new zircon U-Pb age and Hf-O isotopic data, the Cretaceous volcanic rocks in this study can further subdivide the corresponding volcanic activity into three major stages: Stage 1 (136–129 Ma; Dashuang, Gaowu, and Xishantou formations), Stage 2 (125–115 Ma; Chawan, Jiuliping, and Guantou formations), and Stage 3 (110–94 Ma; Chaochuan, Tangshang, and Xiaoxiong formations) from the upper volcanic series.

Zircons (ca. 136–129 Ma) from Stage 1 volcanic rocks have large variations in Hf-O isotopic

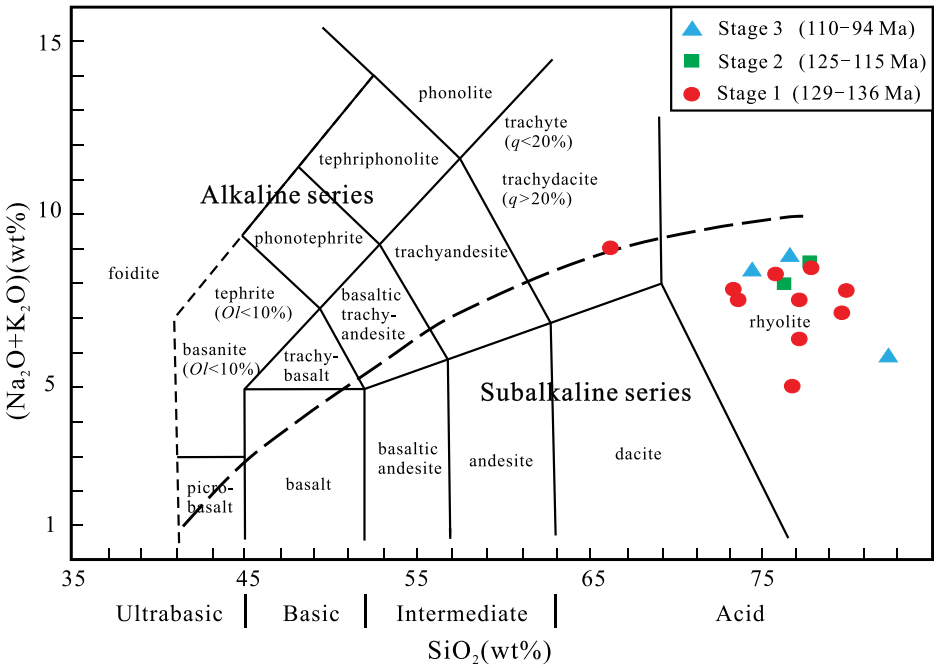

Figure 7. Total alkali versus silica diagram (after Le Maitre et al., 1989; with the dashed line from Irvine and Baragar, 1971). MSWD—mean square weighted deviation.

compositions, with relatively low $\varepsilon_{Hf}(t)$ (–15.6 to –1.7), high $\delta^{18}O$ values (5.1–7.5‰), and high $T_{DM2}(Hf)$ (2.17–1.29 Ga) (Figs. 9A–9F). Several older zircons (ca. 171–139 Ma) from this stage have similar $\varepsilon_{Hf}(t)$ (–15.6 to –9.2), $\delta^{18}O$ values (5.6–7.4‰), and $T_{DM2}(Hf)$ (2.17–1.78 Ga), which could be inherited zircons (Figs. 9A–9F).

Compared to Stage 1, zircons (ca. 125–115 Ma) from Stage 2 volcanic rocks also have a wide range of Hf-O isotopic compositions, but with much higher $\varepsilon_{Hf}(t)$ (–12.4 to +2.6), lower $\delta^{18}O$ values (4.3–6.6‰), and lower $T_{DM2}(Hf)$ (1.96–1.01 Ga) (Figs. 9G–9L). Several older zircons (153–127 Ma) from this stage record similar $\varepsilon_{Hf}(t)$ (–9.2 to –3.6), $\delta^{18}O$ values (4.6–6.0‰), and higher $T_{DM2}(Hf)$ (1.78–1.41 Ga), which could be also inherited zircons (Figs. 9G–9L). In addition, two older zircons (200 and 145 Ma) from this stage have much lower $\varepsilon_{Hf}(t)$ (–11.9 to –11.0), $\delta^{18}O$ values (5.1–6.3‰), and higher $T_{DM2}(Hf)$ (1.99–1.89 Ga) (Figs. 9I and 9J), which could be xenocrysts.

The Stage 3 (ca. 110–94 Ma) zircons show almost uniform Hf-O isotopic compositions, with high $\varepsilon_{Hf}(t)$ (–6.3 to –2.0), low $\delta^{18}O$ values (4.5‰–5.7‰), and low $T_{DM2}(Hf)$ (1.56–1.29 Ga) (Figs. 9M–9R). Two older zircons (129–125 Ma) have similar Hf-O isotopic compositions with $\varepsilon_{Hf}(t)$, $\delta^{18}O$ values, and $T_{DM2}(Hf)$ of –4.1 to –3.2, 4.8–5.1‰, and 1.38–1.44 Ga, respectively, which could be inherited zircons (Figs. 9M–9R). Some older zircons (116–156 Ma) from this stage have obvious lower $\varepsilon_{Hf}(t)$ (–13.3 to –8.1), variable $\delta^{18}O$ values (1.7–6.0‰), and older $T_{DM2}(Hf)$ (2.03–1.69 Ga), which could be xenocrysts (Figs. 9M–9R).

6. DISCUSSION

6.1. Origins of the Cretaceous Volcanic Rocks

Most samples from the Cretaceous volcanic rocks are rhyolitic rocks that have high SiO_2 (72–81 wt%) and low Mg# values (15.9–42.9) (Table S3), suggesting that they were unlikely directly formed by fractional crystallization of basaltic magma. In addition, the samples have relatively low Nb/U (3.4–9.1) and Ce/Pb (1.5–6.7) ratios which are similar to those of the average continental crust (Nb/U = 6.2, Ce/Pb = 3.9; Rudnick and Fountain, 1995), but significantly lower than those of mid-ocean ridge and ocean island basalts (Nb/U = 47 ± 10 and Ce/Pb = 25 ± 5; Hofmann et al., 1986), supporting their crustal origin.

Zircon Hf isotopic data can place robust qualitative constraints on the origins of magmatic rocks (Belousova et al., 2006). Significant Hf-isotope variations could be generated either by the decoupled release of zircon Hf and non-zircon Hf from a single crust-derived magma

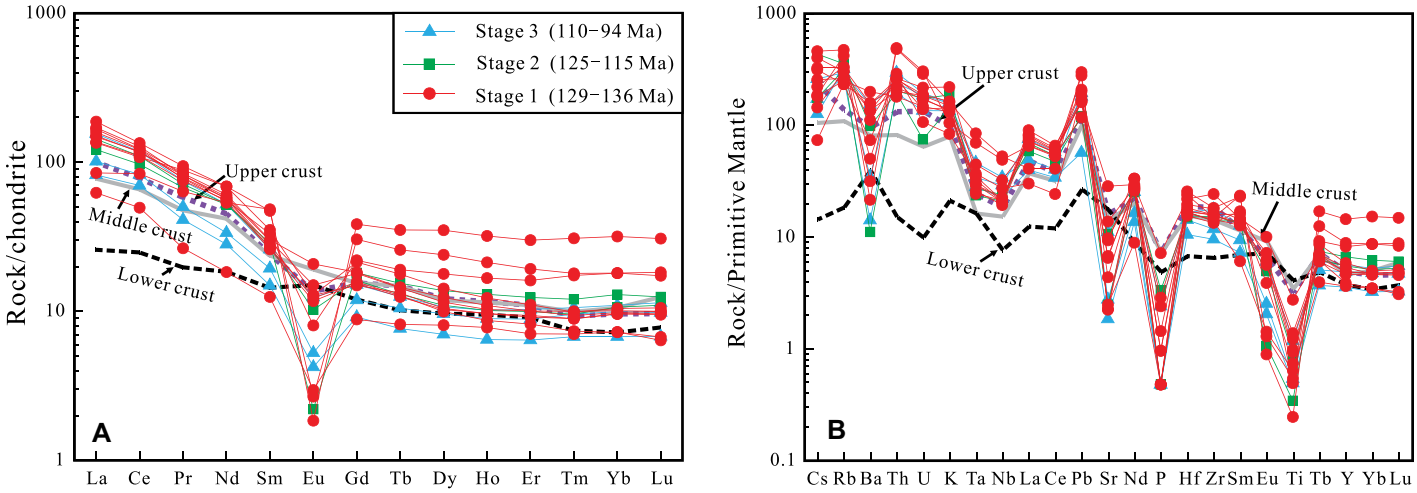

Figure 8. Chondrite-normalized rare earth element (A; normalization values from Boynton, 1984) and primitive mantle-normalized multi-element patterns (B; normalization values from McDonough and Sun, 1995) for the volcanic rocks in SE Zhejiang Province, China.

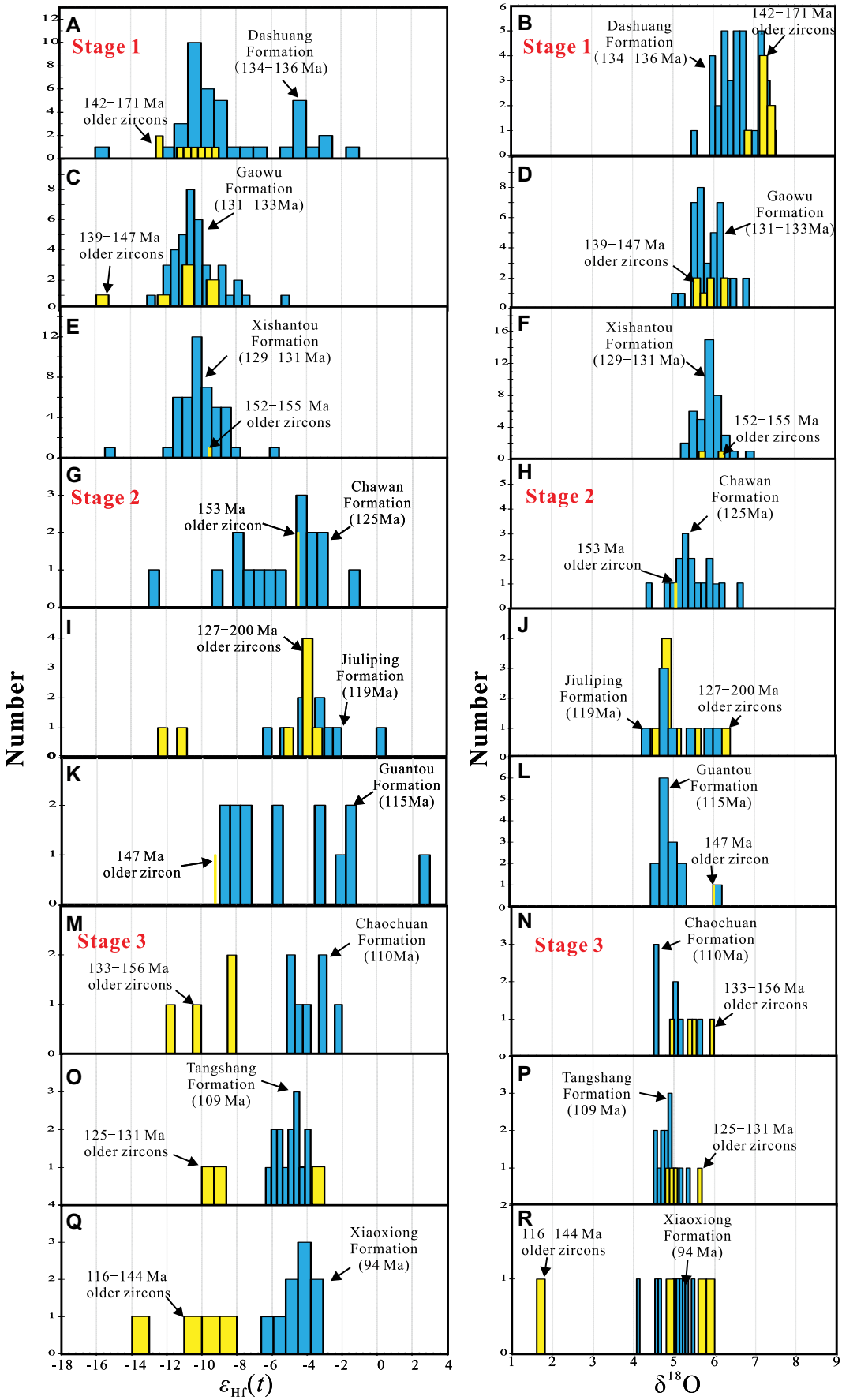

Figure 9. Histograms of (A, C, E, G, I, K, M, O, and Q) $\varepsilon_{Hf}(t)$ and (B, D, F, H, J, L, N, P, and R) $\delta^{18}O$ values of zircons from the representative volcanic rocks in SE Zhejiang Province, China.

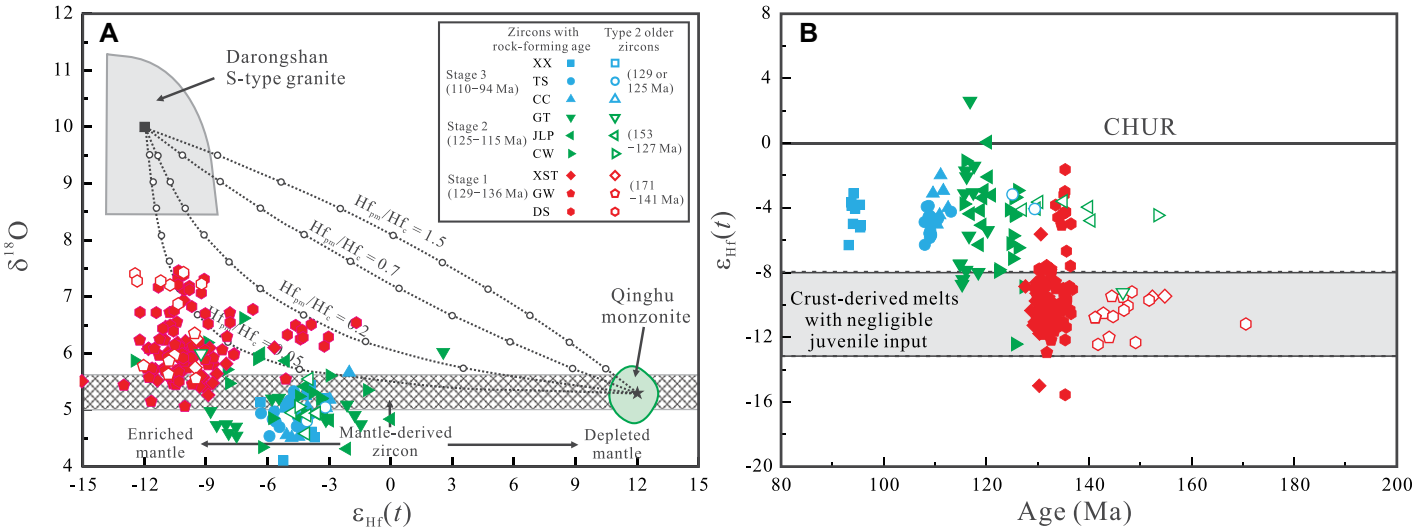

Figure 10. Diagram of (A) $\delta^{18}O$ versus $\varepsilon_{Hf}(t)$ (modified after Li et al., 2009) and (B) $\varepsilon_{Hf}(t)$ versus U-Pb ages (modified after Liu et al., 2016) for zircons from the representative volcanic rocks in SE Zhejiang Province, China. Dotted lines denote the two-component mixing trends between mantle- and crust-derived magmas. Hf_{pm}/Hf_c is the ratio of Hf concentration in parental mantle magma over crustal melt. The shaded area shows isotopic compositions of ancient crust-derived melts with negligible juvenile input (Liu et al., 2014b; Xu et al., 2007). CHUR—chondritic uniform reservoir. XX—the Xiaoxiong Formation; TS—the Tangshan Formation; CC—the Chaochuan Formation; GT—the Guantou Formation; JLP—the Jiuliping Formation; CW—the Chawan Formation; XST—the Xishantou Formaiton; GW—the Gaowu Formation; DS—the Dashuang Formation.

source (Tang et al., 2014) or by mixing of magmas from different sources (Griffin et al., 2002; Kemp et al., 2007). Zircons are highly retentive of the magmatic O isotopic compositions (Kemp et al., 2007; Li et al., 2009), and those in equilibrium with mantle-derived magmas have very consistent $\delta^{18}O$ values of (5.3 ± 0.6‰, 2σ) (Valley et al., 2005). The zircon O isotopes are insensitive to magmatic differentiation (Li et al., 2009), and uncertainty by SIMS in situ zircon O-isotope analysis is limited (1σ = 0.1–0.2‰) (Tang et al., 2015). Therefore, high $\delta^{18}O$ igneous rocks (>6‰) are indicative of the incorporation of recycled supracrustal components, whereas low $\delta^{18}O$ igneous rocks ($\delta^{18}O$ < 5‰) require high-temperature altered rocks by seawater ($\delta^{18}O$ = 0‰) or meteoric water ($\delta^{18}O$ < 0‰) in their petrogenesis (Bindeman and Serebryakov, 2011; Bindeman and Valley, 2001). In this study, only zircons with concordant ages are used to constrain the origins and evolutions of volcanic rocks, to rule out the influence of hydrothermal alteration of metamict zircons (Zhao et al., 2013).

6.1.1. Stage 1 Volcanic Rocks Produced by Reworking of Continental Crust

The Stage 1 volcanic rocks (136–129 Ma) show large variable zircon Hf and O isotopic compositions with multi-peak distributions (Figs. 9A–9F), implying that different sources were probably involved in their formation. Most zircons have high $\delta^{18}O$ (6.0–7.5‰) and variable negative $\varepsilon_{Hf}(t)$ (–12.2 to –1.7) values (Fig. 10), with bimodal distribution in two-stage Hf model ages (1.3–2.0 Ga), indicating that their parental magma was most probably produced by partial melting of both ancient and juvenile continental supracrustal rocks, including (meta)sedimentary and altered (meta)volcanic rocks (Valley et al., 2005). Some zircons have mantle-like $\delta^{18}O$ (5.1–6.0‰) but also show strong negative $\varepsilon_{Hf}(t)$ values (–15.0 to –5.1), implying that ancient (1.5–2.1 Ga) igneous rocks from the continental lower crust were involved in their petrogenesis. The Stage 1 volcanic rocks display wide variations of rare-earth elemental and trace elemental concentrations (Fig. 8), which are overlapped with those either from the continental lower or middle-upper crust (Rudnick and Gao, 2003), supporting the above interpretation. Consequently, the Stage 1 volcanic rocks in this study were derived from the Meso- to Paleo-Proterozoic (1.3–2.1 Ga) continental crustal materials.

6.1.2. Stage 2 and 3 Volcanic Rocks Formed by Reworking of Juvenile Continental Crust

The Stage 2 volcanic rocks (125–115 Ma) also have large variable $\varepsilon_{Hf}(t)$ (–12.4 to +2.6) and $\delta^{18}O$ values (4.3‰ to 6.6‰), reflecting different sources. Compared with the Stage 1 volcanic rocks, the majority of magmatic zircons from the Stage 2 volcanic rocks have preserved mantle-like $\delta^{18}O$ values, and relatively higher $\varepsilon_{Hf}(t)$ values (>–9, with the peak of about –4) (Fig. 9). Generally, igneous rocks that are differentiated from mantle-derived magmas or produced by melting of juvenile mafic crust tend to crystallize zircons with mantle-like $\delta^{18}O$ values (Valley et al., 1998; Zhao et al., 2013). Considering their crustal origin discussed above, we suggest these volcanic rocks were mainly derived from partial melting of juvenile lower crust materials. Some magmatic zircons show high $\delta^{18}O$ (up to 6.6‰) with low $\varepsilon_{Hf}(t)$ values (lower to –12.4), similar to those of Stage 1 volcanic rocks, indicating some supracrustal materials were also assimilated to their magmas. Overall, we consider that the sources of Stage 2 volcanic rocks are mainly juvenile lower crust with some of the supracrustal materials.

As shown in Figure 10A, a high proportion of zircon grains in Stage 2 volcanic rocks with low $\delta^{18}O$ values plot significantly below the range of mantle-like values. Low-$\delta^{18}O$ zircons probably crystallized from melts that were assimilated significant amounts of high-temperature hydrothermally altered crustal material either at shallow crustal levels or deep in the crust, or differentiation from a low-$\delta^{18}O$ mantle source (Monani and Valley, 2001; Troch et al., 2019). High-temperature water-rock interaction depletes ^{18}O of the rocks (Bindeman and Serebryakov, 2011), which are generally found in continental rifts or calderas environments with high magma and heat fluxes (Bindeman et al., 2014; Wang et al., 2011b). SE China was an active continental margin during the Mesozoic period due to the subduction of the paleo-Pacific plate (Zhou et al., 2006). In addition, low-$\delta^{18}O$ wall rocks have not

been identified in this region (Gao et al., 2018; Zou et al., 2021). Thus, the low-$\delta^{18}O$ zircons in this study were unlikely to have resulted from the assimilation of low-$\delta^{18}O$ wall rocks. Partial melting of hydrothermally altered oceanic crust is an alternative way to generate low-$\delta^{18}O$ magmas (Wei et al., 2002). Low-$\delta^{18}O$ zircons from the Stage 2 volcanic rocks have variable and negative $\varepsilon_{Hf}(t)$ values (–8.8 to 0), which are inconsistent with the origin entirely derived from a hydrothermally altered oceanic crust with uniform and positive $\varepsilon_{Hf}(t)$ values (Xue et al., 2018). However, the involvement of some altered oceanic crust-derived melts for their origin could be possible, while the signature exhibiting variable and negative $\varepsilon_{Hf}(t)$ values can be explained by the mixing of continental crust-derived melts. These zircon grains do not contain any conspicuous fractures, inclusions, or alteration, with "normal" U concentrations (between 130 and 956 ppm; Table S2), and thus could not be resulted from metamictization and recrystallization promoted by the presence of water-saturated, volatile-rich magmas in the final stage of magmatic differentiation (Gao et al., 2018). There are several likely causes to generate low-$\delta^{18}O$ zircons in the current situation as below: (1) the supracrustal materials with low-$\delta^{18}O$ values were produced from hydrothermal systems initiated by the older magmatic pulses, subsequently, the newly magmas triggered partial remelting of the hydrothermally altered differentiates leading to the formation of low-$\delta^{18}O$ melts (Wotzlaw et al., 2012); (2) involvement of some altered oceanic crust derived melts to produce low-$\delta^{18}O$ magmas (Hart et al., 1999); and (3) remelting of the juvenile crustal materials with low-$\delta^{18}O$ values, which were generated by underplating of the sub-arc mantle into the lower crust (Liu et al., 2014a).

Stage 3 (110–94 Ma) volcanic rocks have homogenous Hf-O isotopic compositions, with identical zircon $\varepsilon_{Hf}(t)$ values (–6.3 to –2.0) and low-$\delta^{18}O$ or mantle like $\delta^{18}O$ values (4.5‰ to 5.7‰), indicating a single magma source region. If the low-$\delta^{18}O$ zircons from the Stage 3 volcanic rocks were generated from the hydrothermally altered differentiates triggered by the hydrothermal system, high-$\delta^{18}O$ zircon derived from supracrustal rocks should also be observed, however, that is not the case. Therefore, we suggest that the low-$\delta^{18}O$ zircons from both Stage 2 and 3 volcanic rocks could be derived from melts of the altered oceanic crust or the juvenile crustal materials. Melts from partial melting of hydrothermally altered oceanic crust seem to have high Sr contents and Sr/Y values (Richards et al., 2012). However, the relatively low Sr contents (37–223 ppm), and low Sr/Y ratios (2.4–9.1) of Stage 3 volcanic samples still could be explained as the products of partial melting of hydrothermally altered ancient oceanic crust buried beneath the lower continental crust (e.g., Gazel et al., 2015).

The Stage 3 volcanic rocks show much lower contents of Cs, Pb, and U (Fig. 8), similar to the typical characteristics dominated by continental lower crust (Rudnick and Gao, 2003). All zircons from Stage 3 have similar Hf-O isotopic compositions to those mantle-like zircons of Stage 2, we thus consider that the sources of Stage 3 volcanic rocks are most likely the juvenile lower crustal materials, and lack supracrustal materials for their origin. Meanwhile, it is still possible that the involvement of melts from partial remelting of pre-existing hydrothermally altered oceanic crust for the formation of these volcanic rocks of Stages 2 and 3.

6.2. Evidence for the Model of Transcrustal Magmatic System

The formation, storage, and differentiation of magma in the crust are of fundamental importance in igneous geology (Jackson et al., 2018). A classic concept for igneous processes is a melt-dominated magma chamber with high-melt fraction commonly in a shallow depth and eventually solidifying (Cooper and Kent, 2014). However, some geophysical, geochemical, and petrological observations are inconsistent with the classic magma chamber model (Cashman et al., 2017). On the one hand, new conceptual models of transcrustal magmatic systems (TCMS) have been increasingly raised (Cashman et al., 2017; Liu and Lee, 2020). The model of TCMS suggests that the magmatic processes are probably associated with a low-melt-fraction "mush reservoir" as a reactive melt flow (Cashman et al., 2017; Liu and Lee, 2020), which evolved through the whole crust during their emplacement (Hepworth et al., 2020; Jackson et al., 2018; Zhang et al., 2018). The emerging consensus is that TCMS are dominated by crystal mush. Mushes are multiphase (crystal-melt-volatile) systems, in which crystals form a continuous framework and melts are distributed. Mushes are at or above the solidus and are synonymous with partially molten rock. Mushes in their entirety are not eruptible because their rheology is controlled by the deformation of the crystalline framework. Mush fragments, however, can be erupted as crystal clots (glomerocrysts), cumulate nodules, or restite. Eruptible magma, by contrast, is defined as a suspension of crystals in the melt (with or without exsolved volatiles).

Herein, special relationships between older zircons and magmatic zircons from each stage of volcanic rocks in this research were hard to explain by the classic magma chamber paradigm. Significantly, two types of older zircons for each of the three volcanic stages could be identified. Type 1 older zircons from each stage show obvious different Hf-O isotopic compositions from those zircons of rock-forming age, which could be xenocrysts assimilated from the country rocks. However, Type 2 older zircons share similar Hf-O isotopic and trace elemental compositions to those magmatic zircons of rock-forming age (autocrysts) within single stages. These similarities may imply a genetic relationship between autocrysts and Type 2 older zircons and suggest that these Type 2 older zircons are likely to be inherited zircons (Zhao et al., 2013). As a whole, volcanic magmatisms from different stages have different Hf-O isotopic and trace elemental compositions. If Type 2 older zircons are all inherited zircons, it is hard to explain the very small intervals (5–15 m.y.) between Type 2 older zircons and zircon autocrysts for each stage of volcanic rock by using the traditional melt-dominated magma chamber model. For example, the Type 2 older zircons (171–139 Ma) from Stage 1 show low $\varepsilon_{Hf}(t)$ values (–15.6 to –9.2, peak at –11) with two groups of $\delta^{18}O$ values (crust-like or mantle-like), which share similar Hf-O isotope compositions with most of Stage 1 (136–129 Ma) zircons (Figs. 9 and 10), and imply that the reworking of ancient continental crustal materials also happened at 171–139 Ma. Consequently, the 171–139 Ma zircons must represent the inherited zircons owing to similar isotopic compositions. However, considering the wide range of Hf-O isotopic compositions, the Stage 1 (136–129 Ma) volcanic rocks could not be directly produced by the reworking of those 171–139 Ma rocks during such a short interval of time. They are in contradiction with the conventional melt-dominated model. Same observations were also recorded from Stage 2 volcanic rocks. Type 2 older zircons (140–127 Ma) from Stage 2 show relatively high $\varepsilon_{Hf}(t)$ values (–4.8 to –3.6) with low-$\delta^{18}O$ or mantle-like $\delta^{18}O$ values (4.6‰ to 5.5‰), and also overlapped with the majority of Stage 2 (125–115 Ma) zircons (Figs. 9 and 10), indicating they are of affinity between the 140–127 Ma melts and the Stage 2 (125–115 Ma) volcanic magmas. We suggest that the Type 2 older zircons could be well explained as antecrysts, which thus have slightly older ages (intervals of 5–15 m.y.) than those of autocrysts within the same volcanic stage, and share similar chemical characteristics.

From the mush-dominated perspective, the Type 2 older zircons in the volcanic rocks could be recycled from an older solidified or partially solidified magma chamber and/or magma mush, representing antecrysts (Davidson et al., 2007; Miller et al., 2007). Because eruption of magma requires low to moderate crystal fraction and

high temperatures (relative to stored crystal mushes), most zircon crystals are more likely to be eradicated during thermal rejuvenation preceding major eruptions (Miller et al., 2007). Therefore, the youngest zircons crystallized in the volcanic rocks (autocrysts) represent the time of the eruption. This model could well explain the zircons of different ages with similar ranges of Hf-O isotopes in our study. Moreover, the compositions of magma mush could also be changed by the changing of magma sources (comparing between Stages 1 and 2) or assimilation of wall rocks during their ascent (comparing between Stages 2 and 3). Type 1 older zircons (156–116 Ma) from Stage 3 show obvious different Hf-O isotope compositions to these autocrysts (110–94 Ma), representing contamination of wall rocks during the migration and ascent of the magma.

Systematically zircon U-Pb geochronological studies of the volcanic sequences from southeastern Zhejiang Province suggest that the late Mesozoic volcanism in this area is long-term and discontinuous (Liu et al., 2014b, 2012a, 2016). The eruption of a large volume of volcanic rocks needs massive magma chambers in the lower crust, which are surprisingly difficult to form and maintain, by use of classic physical models based on thermal, mechanical, and dynamical principles (Cashman et al., 2017). Meanwhile, high rates of melt transfer are required to maintain melt-dominated magma bodies at shallower levels in the crust, which are also hard to satisfy. By contrast, the long-lived cooler non-eruptible mushes can easily develop throughout the crust (Cashman et al., 2017). The protoliths (magma mushes) of the volcanic rocks were still relatively hot and partially solidified, which could be easily reactivated by any exotic source of heat (such as an influx of magma, heat, fluid, and/or volatiles).

As discussed above, either continental lower or middle-upper crustal materials were involved as magmatic sources for a single main volcanic eruption in Zhejiang Province, such as Stages 1 and 2 volcanic rocks. We thus suggest that such a mush-dominated model requires connecting their processes throughout the transcrustal magma systems (TCMS) (Fig. 11), which is in agreement with recent studies in this area (Xu et al., 2021; Zhang et al., 2018). The long-lived magmatic systems may extend beneath lower crustal magma reservoirs (Fig. 11), maintained and recharged by a discontinuous contribution of synchronous underplated mantle-derived magmas (Xu et al., 2021), which could also provide a reasonable explanation for the changing of magma sources for different stages of volcanic activity. In addition, previous studies based on geophysics and petrology suggest that there may be a high velocity and density mafic layer underneath SE China, which is considered as an intrusive result of mafic underplated at the base of the continental crust (Xu et al., 1996, 1999). Numerous layered reflectors beneath the coastal terrane (interpreted as Cretaceous mafic sills), also support large volumes of mantle-derived material into the crust due to the magmatic underplating (Dong et al., 2020).

From a TCMS viewpoint (Fig. 11), magma mushes originated from partial melting of the lower crust by mafic underplating, were transferred to the middle-upper crust, then developed by mixed with melts and/or crystals from the middle-upper crust, and finally erupted to form Stage 1 volcanic rocks. After the eruption, residual and new mushes were gradually accumulated in shallow chambers by the replenishment of magma mushes from lower-crustal reservoirs (juvenile lower crust), involving some supracrustal materials, and ultimately formed Stage 2 volcanic rocks. By sweeping crustal materials both in the shallow and deeper chambers, the magma mushes for Stage 3 volcanic rocks were dominantly coming from the juvenile continental crust. Similar principles can apply to the origin of Stage 2 volcanic rocks by sweeping the most ancient lower-crustal materials from the deeper reservoirs.

6.3. Relationship with the Paleo-Pacific Plate Subduction

It is generally accepted that the Cretaceous volcanic series in SE China were related to the subduction of the paleo-Pacific oceanic plate (Guo et al., 2021; Li et al., 2014a; Liu et al., 2014b, 2012a; Xu et al., 2021). Wang et al. (2011a) showed that the igneous rocks with intrusion ages between 180 and 125 Ma generally become progressively younger toward the northeast in SE China, which was interpreted by southwestward oblique subduction of the paleo-Pacific plate. From the zircon U-Pb ages of lower volcanic series in Zhejiang Province, a similar trend of younging toward the northeast has been also recognized during 145–127 Ma (Fig. 2) (Liu et al., 2020, 2016). These observations allow us to speculate that southwestward subduction was followed by a northeastward rollback of the paleo-Pacific plate during 145–127 Ma (Liu et al., 2018). As suggested by most previous studies, the paleo-Pacific plate was moving toward the northwest during 110–83 Ma, with evidence of the abundance of contemporary extension-related rocks (He and Xu, 2012; Jiang et al., 2015; Li et al., 2014b, 2014d, 2016). Remarkably, the entire upper volcanic series in SE China was generated at 110–88 Ma and mainly concentrated in the coastal area (Fig. 2) (Liu et al., 2016), consistent with this view. Thus, the direction of motion of the paleo-Pacific plate has been suggested to have changed during the period 127–110 Ma (Liu et al., 2018; Sun et al., 2007).

Consequently, the Stages 1–3 volcanic rocks (136–129 Ma, 125–115 Ma, 110–94 Ma) were produced at different tectonic settings, respectively, in response to the changing of the motion direction of the subducting paleo-Pacific plate. The northeastward younging trend of Stage 1 (136–129 Ma) volcanic rocks together with other Early Cretaceous volcanic rocks of SE China, evidently indicates the roll-back of the paleo-Pacific southwest-directed subduction. Stage 1 volcanic rocks were generated by the eruption of magma mushes (derived from the reworking of continental lower and middle-upper crust), caused by the reduced pressure in response to the rollback of the paleo-Pacific plate, and heat sources provided by underplating and intraplating (Zhou and Li, 2000). Stage 2 volcanic rocks were produced by the subsequent eruption of magma mushes (originate from the juvenile lower crust and ancient upper crustal materials). During this "golden transformation" period (Sun et al., 2007), the zircon $\varepsilon_{Hf}(t)$ values of volcanic rocks increase gradually, while zircon $\delta^{18}O$ values decrease gradually following

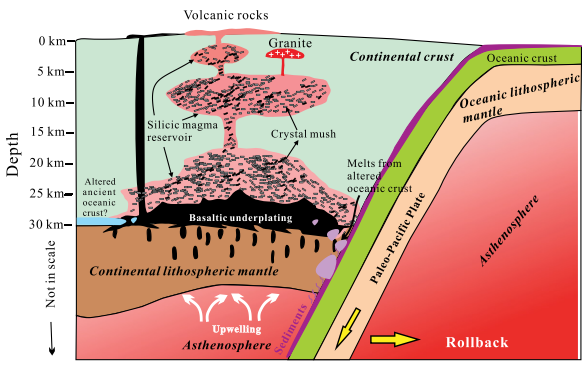

Figure 11. Diagrammatical volcanic genetic model showing the Cretaceous transcrustal magmatic system in SE China (adapted from Xu et al., 2021). Lower-crust-derived melt induced by underplating of mantle-derived mafic magma ascended to form deep silicic magma reservoirs in the middle- to upper-crust, which feeds and recharges the shallow crustal magma reservoirs. See text for a detailed discussion.

the younging of the crystallization age. It is plausible that Stage 2 magmatism was related to the continued rollback of the paleo-Pacific plate and the outboard retreat of its subduction zone (Liu et al., 2014b, 2012a; Wang et al., 2017). Stage 3 volcanic rocks could be the final products of magma mushes (juvenile lower crustal materials), triggered by the roll-back of the paleo-Pacific northwest-directed subduction, showing even higher $\varepsilon_{Hf}(t)$ values and lower $\delta^{18}O$ values of zircon. It is worth noting that the low-$\delta^{18}O$ signatures have been just observed from Stages 2 and 3 magmatisms, corresponding to the roll-back-tearing of the paleo-Pacific Ocean (Guo et al., 2021). Such zircon Hf-O isotopic variation trends reflect that the chemical and isotopic compositions of the melting sources for the Cretaceous volcanic rocks became similar (mainly the juvenile lower crust materials). Our new results indicate that the pre-existing deep crustal materials were gradually modified and replaced by the newly accreted arc crust as a result of the paleo-Pacific plate subduction.

Two basic categories of magma types, i.e., cold-wet-oxidized in subduction zones or hot-dry-reduced in areas of mantle-upwelling settings were proposed by Bachmann and Bergantz (2008). The former types show pronounced U-shaped REE patterns with slightly negative Eu anomalies, whereas the latter types are characterized by seagull-like REE patterns and significant negative Eu anomalies (Yan et al., 2018). A continuum of magmatic compositions between the cold-wet-oxidized and hot-dry-reduced magma types can be observed for Stages 1–3 volcanic rocks (Fig. 8), which are also consistent with a previously proposed geodynamic model from a subduction-compressional to an extensional regime as a response to rollback subduction of the paleo-Pacific plate (He and Xu, 2012; Liu et al., 2014b). Rollback of the subducting plate can generate long-term crustal extension with the development of high heat flow in back-arcs (Yan et al., 2018).

More importantly, the oxygen fugacities ($\log fO_2$) of Stages 1–3 volcanic rocks change systematically, also providing the direct relationship between volcanic and subduction. We used a calibration method of Smythe and Brenan (2016) to estimate oxygen fugacity ($\log fO_2$) based on zircon, which depends on the temperature, Ce^{3+}/Ce^{4+} ratio of the melt and water content. In this method, the temperature of the melt was obtained using the Ti-in-zircon thermometer (Ferry and Watson, 2007). The Ce^{3+}/Ce^{4+} ratios of the melts were calculated using a lattice strain model (Ballard et al., 2002). The H_2O concentration of 4 wt% was assumed by considering the mean water contents of arc magmas (Plank et al., 2013). The Stage 1 volcanic rocks show significant variations of oxygen fugacities ($\log fO_2$), reflecting the involvement of different sources in their formation (Fig. 12A). By contrast, the oxygen fugacities ($\log fO_2$) from Stages 2 and 3 volcanic rocks gradually increase, which likely requires an increase in the amounts of dehydration-released fluids, and favor the increase of the intensity of retreating subduction (Gerya et al., 2008). Moreover, vanadium is more incompatible with ferromagnesian minerals under high-oxygen-fugacity conditions, so V content relative to those of other transition metals (e.g., Sc) can be also used as a qualitative proxy for fugacity (Zhu et al., 2016). The lowest V/Sc ratios recorded by Stage 2 volcanic rocks (0.4–0.5) relative to those from Stage 3 volcanic rocks (1.0–1.5), also support this speculation. Zircon Th/U ratios have been applied to track varying tectonic stress regimes, with lower values (<1.0) representing compression and higher values for extension (McKay et al., 2018). The zircon Th/U values from Stages 1 and 2–3 volcanic rocks regularly increase (Fig. 12B), which also reflect a transition from compressional to the extensional environment, and favor our above interpretation. Overall, we think the predominant driving forces for those volcanic activities and long-lived transcrustal magmatic systems are responding to the change of Pacific plate motion beneath Southeast China. Of course, the intrusive counterparts are indispensable parts of the TCMS, which have been referred to recently (Cashman et al., 2017; Chen et al., 2021; Wu et al., 2017), and need to be further studied in the future.

7. CONCLUSIONS

The Cretaceous volcanic rocks in southeastern Zhejiang Province were produced mainly at three episodes: 136–129 Ma, 125–115 Ma, and 110–94 Ma. The zircon Hf-O isotopic results indicate that the pre-existing ancient crustal materials were gradually replaced by the juvenile lower crustal materials as the main melting sources for the Cretaceous volcanic rocks. The sources of Stage 1 (136–129 Ma) volcanic magmas are mainly ancient continental lower and middle-upper crustal materials. The sources of

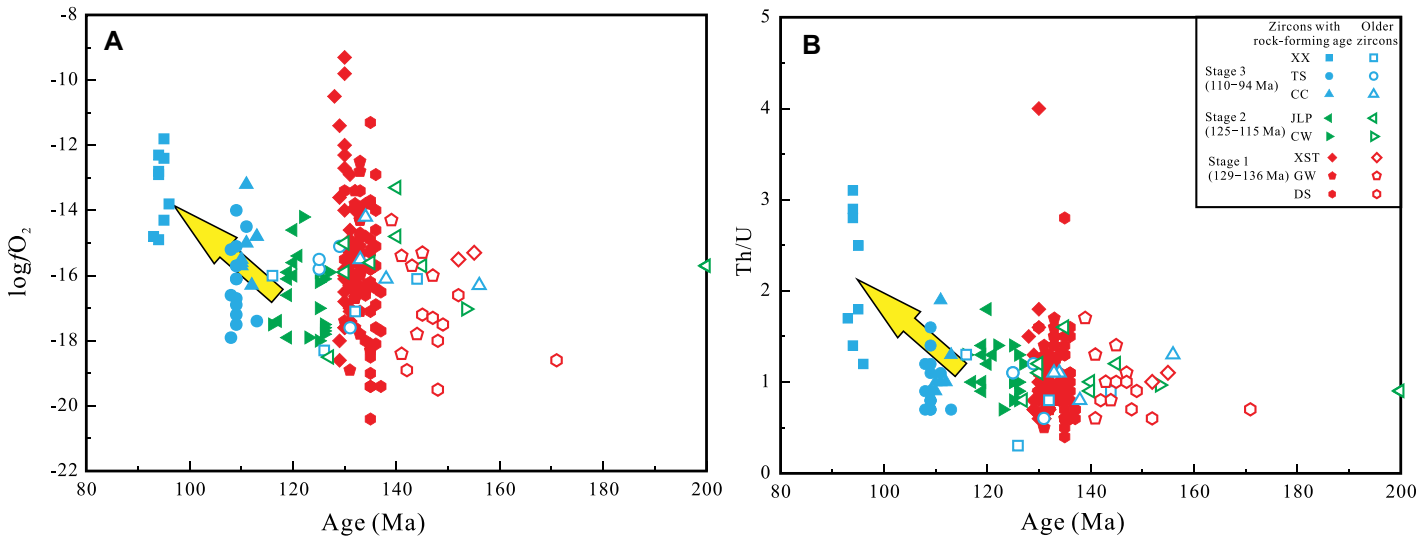

Figure 12. Diagrams showing zircon (A) logfO_2 and (B) Th/U versus U-Pb age from the representative volcanic rocks in SE Zhejiang Province, China. XX—the Xiaoxiong Formation; TS—the Tangshan Formation; CC—the Chaochuan Formation; GT—the Guantou Formation; JLP—the Jiuliping Formation; CW—the Chawan Formation; XST—the Xishantou Formaiton; GW—the Gaowu Formation; DS—the Dashuang Formation.

Stage 2 volcanic magmas are mainly juvenile lower crust with some supracrustal materials. The sources of Stage 3 volcanic magmas are most likely the juvenile lower crustal materials and lack of supracrustal materials for their origin. The Cretaceous volcanic rocks in southeastern Zhejiang Province were derived from the long-lived transcrustal magmatic systems, dominated by crystal mush, maintained and recharged by a discontinuous contribution of contemporaneous underplated mantle-derived magmas, instead of melt-dominated magma chambers. Systematical changes such as oxygen fugacity and tectonic regime were recorded from those volcanic rocks, providing the direct relationship between volcanic and subduction. The most possible driving forces for those volcanic activities and long-lived transcrustal magmatic systems originated from the change of Pacific plate motion beneath Southeast China.

ACKNOWLEDGMENTS

We are grateful for the constructive reviews by Science Editor Wen-Jiao Xiao, Associate Editor Lai-Shi Zhao, and three anonymous reviewers. This research was financially supported by the National Key R&D Program of China (no. 2016YFC0600405). Additional support was provided from the National Science Foundation of China (grant No. 42073046), the Innovation and Entrepreneurship Funding of High-Level Overseas Talents of Guizhou Province (Jie-Hua Yang, [2020]03), CAS "Light of West China" Program (Jie-Hua Yang), and Youth Innovation Promotion Association, Chinese Academy of Sciences (no. 2020393). We greatly thank Dr. Xiao-Ping Xia, Dr. Yan-Wen Tang, and Dr. You-Wei Chen for their help with analyses and technical assistance. Jun-Hong Zhao is thanked for providing constructive comments on the earlier version of the paper.

REFERENCES CITED

Bachmann, O., and Bergantz, G.W., 2008, Rhyolites and their source mushes across tectonic settings: Journal of Petrology, v. 49, no. 12, p. 2277–2285, https://doi.org/10.1093/petrology/egn068.

Ballard, J.R., Palin, M.J., and Campbell, I.H., 2002, Relative oxidation states of magmas inferred from Ce(IV)/Ce(III) in zircon: Application to porphyry copper deposits of northern Chile: Contributions to Mineralogy and Petrology, v. 144, no. 3, p. 347–364, https://doi.org/10.1007/s00410-002-0402-5.

Belousova, E.A., Griffin, W.L., and O'Reilly, S.Y., 2006, Zircon crystal morphology, trace element signatures and Hf isotope composition as a tool for petrogenetic modelling: Examples from eastern Australian granitoids: Journal of Petrology, v. 47, no. 2, p. 329–353, https://doi.org/10.1093/petrology/egi077.

Bindeman, I.N., and Serebryakov, N.S., 2011, Geology, Petrology and O and H isotope geochemistry of remarkably ^{18}O depleted Paleoproterozoic rocks of the Belomorian Belt, Karelia, Russia, attributed to global glaciation 2.4 Ga: Earth and Planetary Science Letters, v. 306, no. 3–4, p. 163–174, https://doi.org/10.1016/j.epsl.2011.03.031.

Bindeman, I.N., and Valley, J.W., 2001, Low-$\delta^{18}O$ Rhyolites from Yellowstone: Magmatic evolution based on analyses of zircons and individual phenocrysts: Journal of Petrology, v. 42, no. 8, p. 1491–1517, https://doi.org/10.1093/petrology/42.8.1491.

Bindeman, I.N., Serebryakov, N.S., Schmitt, A.K., Vazquez, J.A., Guan, Y., Azimov, P.Y., Astafiev, B.Y., Palandri, J., and Dobrzhinetskaya, L., 2014, Field and microanalytical isotopic investigation of ultradepleted in ^{18}O Paleoproterozoic "Slushball Earth" rocks from Karelia, Russia: Geosphere, v. 10, no. 2, p. 308–339, https://doi.org/10.1130/GES00952.1.

Boynton, W.V., 1984, Geochemistry of the rare earth elements: Meteorite studies, *in* Henderson, P., ed., Rare Earth Elements Geochemistry: Amsterdam, Netherlands, Elsevier, https://doi.org/10.1016/B978-0-444-42148-7.50008-3.

Cashman, K.V., Sparks, R.S., and Blundy, J.D., 2017, Vertically extensive and unstable magmatic systems: A unified view of igneous processes: Science, v. 355, no. 6331, https://doi.org/10.1126/science.aag3055.

Chen, C.H., Lee, C.Y., Lu, H.Y., and Hsieh, P.S., 2008, Generation of Late Cretaceous silicic rocks in SE China: Age, major element and numerical simulation constraints: Journal of Asian Earth Sciences, v. 31, no. 4–6, p. 479–498, https://doi.org/10.1016/j.jseaes.2007.08.002.

Chen, C.H., Lee, C.Y., and Shinjo, R., 2016, The epilog of the western paleo-Pacific subduction: Inferred from spatial and temporal variations and geochemistry of the Late Cretaceous to Early Cenozoic silicic magmatism in coastal South China: Journal of Asian Earth Sciences, v. 115, p. 520–546, https://doi.org/10.1016/j.jseaes.2015.10.002.

Chen, J.Y., Yang, J.H., Zhang, J.H., and Zhu, Y.S., 2021, Construction of a highly silicic upper crust in southeastern China: Insights from the Cretaceous intermediate-to-felsic rocks in eastern Zhejiang: Lithos, https://doi.org/10.1016/j.lithos.2021.106012.

Cooper, K.M., and Kent, A.J., 2014, Rapid remobilization of magmatic crystals kept in cold storage: Nature, v. 506, no. 7489, p. 480–483, https://doi.org/10.1038/nature12991.

Davidson, J.P., Morgan, D.J., Charlier, B.L.A., Harlou, R., and Hora, J.M., 2007, Microsampling and isotopic analysis of igneous rocks: Implications for the study of magmatic systems: Annual Review of Earth and Planetary Sciences, v. 35, no. 1, p. 273–311, https://doi.org/10.1146/annurev.earth.35.031306.140211.

Dong, S., Li, J., Cawood, P.A., Gao, R., Zhang, Y., and Xin, Y., 2020, Mantle influx compensates crustal thinning beneath the Cathaysia Block, South China: Evidence from SINOPROBE reflection profiling: Earth and Planetary Science Letters, v. 544, https://doi.org/10.1016/j.epsl.2020.116360.

Ferry, J.M., and Watson, E.B., 2007, New thermodynamic models and revised calibrations for the Ti-in-zircon and Zr-in-rutile thermometers: Contributions to Mineralogy and Petrology, v. 154, no. 4, p. 429–437, https://doi.org/10.1007/s00410-007-0201-0.

Gao, Y.Y., Griffin, W.L., Chu, M.F., O'Reilly, S.Y., Pearson, N.J., Li, Q.L., Liu, Y., Tang, G.Q., and Li, X.H., 2018, Constraints from zircon Hf-O-Li isotopic compositions on the genesis of slightly low-$\delta^{18}O$ alkaline granites in the Taohuadao area, Zhejiang Province, SE China: Journal of Asian Earth Sciences, v. 167, p. 197–208, https://doi.org/10.1016/j.jseaes.2017.07.025.

Gazel, E., Hayes, J.L., Hoernle, K., Kelemen, P., Everson, E., Holbrook, W.S., Hauff, F., van den Bogaard, P., Vance, E.A., Chu, S., Calvert, A.J., Carr, M.J., and Yogodzinski, G.M., 2015, Continental crust generated in oceanic arcs: Nature Geoscience, v. 8, no 4, p. 321–327, https://doi.org/10.1038/ngeo2392.

Gerya, T.V., Connolly, J.A.D., and Yuen, D.A., 2008, Why is terrestrial subduction one-sided?: Geology, v. 36, no. 1, https://doi.org/10.1130/G24060A.1.

Gilder, S.A., Keller, G.R., Luo, M., and Goodell, P.C., 1991, Eastern Asia and the Western Pacific timing and spatial distribution of rifting in China: Tectonophysics, v. 197, no. 2–4, p. 225–243, https://doi.org/10.1016/0040-1951(91)90043-R.

Griffin, W.L., Wang, X., Jackson, S.E., Pearson, N.J., O'Reilly, S.Y., Xu, X.S., and Zhou, X.M., 2002, Zircon chemistry and magma mixing, SE China: In-situ analysis of Hf isotopes, Tonglu and Pingtan igneous complexes: Lithos, v. 61, no. 3–4, p. 237–269, https://doi.org/10.1016/S0024-4937(02)00082-8.

Griffin, W.L., Pearson, N.J., Belousova, E.A., and Saeed, A., 2007, Reply to "Comment to short-communication 'Comment: Hf-isotope heterogeneity in zircon 91500' by W.L. Griffin, N.J. Pearson, E.A. Belousova and A. Saeed (Chemical Geology 233 (2006), p. 358–363)" by F. Corfu: Chemical Geology, v. 244, no. 1–2, p. 354–356, https://doi.org/10.1016/j.chemgeo.2007.06.023.

Guo, F., Fan, W., Li, C., Zhao, L., Li, H., and Yang, J., 2012, Multi-stage crust-mantle interaction in SE China: Temporal, thermal and compositional constraints from the Mesozoic felsic volcanic rocks in eastern Guangdong–Fujian provinces: Lithos, v. 150, p. 62–84, https://doi.org/10.1016/j.lithos.2011.12.009.

Guo, F., Wu, Y., Zhang, B., Zhang, X., Zhao, L., and Liao, J., 2021, Magmatic responses to Cretaceous subduction and tearing of the paleo-Pacific Plate in SE China: An overview: Earth-Science Reviews, v. 212, https://doi.org/10.1016/j.earscirev.2020.103448.

Hart, S.R., Blusztajn, J., Dick, H.J.B., Meyer, P.S., and Muehlenbachs, K., 1999, The fingerprint of seawater circulation in a 500-meter section of ocean crust gabbros: Geochimica et Cosmochimica Acta, v. 63, no. 23–24, p. 4059–4080, https://doi.org/10.1016/S0016-7037(99)00309-9.

He, Z.Y., and Xu, X.S., 2012, Petrogenesis of the Late Yanshanian mantle-derived intrusions in southeastern China: Response to the geodynamics of paleo-Pacific plate subduction: Chemical Geology, v. 328, p. 208–221, https://doi.org/10.1016/j.chemgeo.2011.09.014.

Hepworth, L.N., Daly, J.S., Gertisser, R., Johnson, C.G., Emeleus, C.H., and O'Driscoll, B., 2020, Rapid crystallization of precious-metal-mineralized layers in mafic magmatic systems: Nature Geoscience, v. 13, no. 5, p. 375–381, https://doi.org/10.1038/s41561-020-0568-3.

Hofmann, A.W., Jochum, K.P., Seufert, M., and White, W.M., 1986, Nb and Pb in oceanic basalts: New constraints on mantle evolution: Earth and Planetary Science Letters, v. 79, no. 1–2, p. 33–45, https://doi.org/10.1016/0012-821X(86)90038-5.

Hsü, K.J., Li, J., Chen, H., Wang, Q., Sun, S., and Şengör, A.M.C., 1990, Tectonics of South China: Key to understanding West Pacific geology: Tectonophysics, v. 183, no. 1–4, p. 9–39, https://doi.org/10.1016/0040-1951(90)90186-C.

Irvine, T.N., and Baragar, W.R.A., 1971, A guide to the chemical classification of the common volcanic rocks: Canadian Journal of Earth Sciences, v. 8, p. 523–548, https://doi.org/10.1139/e71-055.

Jackson, M.D., Blundy, J., and Sparks, R.S.J., 2018, Chemical differentiation, cold storage and remobilization of magma in the Earth's crust: Nature, v. 564, no. 7736, p. 405–409, https://doi.org/10.1038/s41586-018-0746-2.

Jiang, Y.H., Wang, G.C., Liu, Z., Ni, C.Y., Qing, L., and Zhang, Q., 2015, Repeated slab advance–retreat of the Palaeo-Pacific plate underneath SE China: International Geology Review, v. 57, no. 4, p. 472–491, https://doi.org/10.1080/00206814.2015.1017775.

Kelemen, P.B., Hanghøj, K., and Greene, A.R., 2013, One view of the geochemistry of subduction-related magmatic arcs, with an emphasis on primitive andesite and lower crust, *in* Holland, H.D., and Turekian, K.K., eds., The Crust. Treatise on Geochemistry [second edition]: Oxford, UK, Elsevier-Pergamon, v. 3, p. 749–806, https://doi.org/10.1016/B0-08-043751-6/03035-8.

Kemp, A.I., Hawkesworth, C.J., Foster, G.L., Paterson, B.A., Woodhead, J.D., Hergt, J.M., Gray, C.M., and Whitehouse, M.J., 2007, Magmatic and crustal differentiation history of granitic rocks from Hf-O isotopes in zircon: Science, v. 315, no. 5814, p. 980–983, https://doi.org/10.1126/science.1136154.

Lapierre, H., Jahn, B.M., Charvet, J., and Yu, Y.W., 1997, Mesozoic felsic arc magmatism and continental olivine tholeiites in Zhejiang Province and their relationship with the tectonic activity in southeastern China: Tectonophysics, v. 274, no. 4, p. 321–338, https://doi.org/10.1016/S0040-1951(97)00009-7.

Le Maitre, R.W., Bateman, P., Dudek, A., Keller, J., Lameyre, J., Le Bas, M.J., Sabine, P.A., Schmid, R., Sorensen, H., Streckeisen, A., Woolley, A.R., and Zanettin, B., 1989, Classification of igneous rocks and glossary of terms: Recommendations of the International Union of Geological Sciences Subcommission on the Systematics of Igneous Rocks: Oxford, UK, Blackwell Scientific.

Li, C.L., Wang, Z.X., Wang, D.X., Cao, W.T., Yu, X.Q., Zhou, G.Z., and Gao, W.L., 2014a, Crust-mantle interaction

triggered by oblique subduction of the Pacific plate: Geochronological, geochemical, and Hf isotopic evidence from the Early Cretaceous volcanic rocks of Zhejiang Province, southeast China: International Geology Review, v. 56, no. 14, p. 1732–1753, https://doi.org/10.1080/00206814.2014.956347.

Li, J.H., Zhang, Y.Q., Dong, S.W., and Johnston, S.T., 2014b, Cretaceous tectonic evolution of South China: A preliminary synthesis: Earth-Science Reviews, v. 134, p. 98–136, https://doi.org/10.1016/j.earscirev.2014.03.008.

Li, S., Suo, Y., Li, X., Zhou, J., Santosh, M., Wang, P., Wang, G., Guo, L., Yu, S., Lan, H., Dai, L., Zhou, Z., Cao, X., Zhu, J., Liu, B., Jiang, S., Wang, G., and Zhang, G., 2019, Mesozoic tectono-magmatic response in the East Asian ocean-continent connection zone to subduction of the Paleo-Pacific Plate: Earth-Science Reviews, v. 192, p. 91–137, https://doi.org/10.1016/j.earscirev.2019.03.003.

Li, X.H., 2000, Cretaceous magmatism and lithospheric extension in Southeast China: Journal of Asian Earth Sciences, v. 18, no. 3, p. 293–305, https://doi.org/10.1016/S1367-9120(99)00060-7.

Li, X., Li, W., Wang, X., Li, Q., Liu, Y., and Tang, G., 2009, Role of mantle-derived magma in genesis of early Yanshanian granites in the Nanling Range, South China: In situ zircon Hf-O isotopic constraints: Science in China. Series D, Earth Sciences, v. 52, no. 9, p. 1262–1278, https://doi.org/10.1007/s11430-009-0117-9.

Li, X.H., Li, W.X., Li, Q.L., Wang, X.C., Liu, Y., and Yang, Y.H., 2010a, Petrogenesis and tectonic significance of the ~850 Ma Gangbian alkaline complex in South China: Evidence from in situ zircon U-Pb dating, Hf-O isotopes and whole-rock geochemistry: Lithos, v. 114, no. 1–2, p. 1–15, https://doi.org/10.1016/j.lithos.2009.07.011.

Li, X., Tang, G., Gong, B., Yang, Y., Hou, K., Hu, Z., Li, Q., Liu, Y., and Li, W., 2013, Qinghu zircon: A working reference for microbeam analysis of U-Pb age and Hf and O isotopes: Chinese Science Bulletin, v. 58, no. 36, p. 4647–4654, https://doi.org/10.1007/s11434-013-5932-x.

Li, X.H., Li, Z.X., and Li, W.X., 2014c, Detrital zircon U-Pb age and Hf isotope constrains on the generation and reworking of Precambrian continental crust in the Cathaysia Block, South China: A synthesis: Gondwana Research, v. 25, no. 3, p. 1202–1215, https://doi.org/10.1016/j.gr.2014.01.003.

Li, X.H., Long, W.G., Li, Q.L., Liu, Y., Zheng, Y.F., Yang, Y.H., Chamberlain, K.R., Wan, D.F., Guo, C.H., Wang, X.C., and Tao, H., 2010b, Penglai zircon megacrysts: A potential new working reference material for microbeam determination of Hf-O isotopes and U-Pb age: Geostandards and Geoanalytical Research, v. 34, no. 2, p. 117–134, https://doi.org/10.1111/j.1751-908X.2010.00036.x.

Li, Z.X., and Li, X.H., 2007, Formation of the 1300-km-wide intracontinental orogen and postorogenic magmatic province in Mesozoic South China: A flat-slab subduction model: Geology, v. 35, no. 2, https://doi.org/10.1130/G23193A.1.

Li, Z., Qiu, J.S., and Yang, X.M., 2014d, A review of the geochronology and geochemistry of Late Yanshanian (Cretaceous) plutons along the Fujian coastal area of southeastern China: Implications for magma evolution related to slab break-off and rollback in the Cretaceous: Earth-Science Reviews, v. 128, p. 232–248, https://doi.org/10.1016/j.earscirev.2013.09.007.

Liu, B., and Lee, C.T., 2020, Large silicic eruptions, episodic recharge, and the transcrustal magmatic system: Geochemistry, Geophysics, Geosystems, v. 21, no. 9, https://doi.org/10.1029/2020GC009220.

Liu, H., Wang, Y., Fan, W., Zi, J., Cai, Y., and Yang, G., 2014a, Petrogenesis and tectonic implications of Late-Triassic high $\varepsilon_{Nd}(t)$-$\varepsilon_{Hf}(t)$ granites in the Ailaoshan tectonic zone (SW China): Science China. Earth Sciences, v. 57, no. 9, p. 2181–2194, https://doi.org/10.1007/s11430-014-4854-z.

Liu, J.X., Wang, S., Wang, X.L., Du, D.H., Xing, G.F., Fu, J.M., Chen, X., and Sun, Z.M., 2020, Refining the spatio-temporal distributions of Mesozoic granitoids and volcanic rocks in SE China: Journal of Asian Earth Sciences, v. 201, https://doi.org/10.1016/j.jseaes.2020.104503.

Liu, L., Xu, X., and Zou, H., 2012a, Episodic eruptions of the Late Mesozoic volcanic sequences in southeastern Zhejiang, SE China: Petrogenesis and implications for the geodynamics of paleo-Pacific subduction: Lithos, v. 154, p. 166–180, https://doi.org/10.1016/j.lithos.2012.07.002.

Liu, L., Xu, X., and Xia, Y., 2014b, Cretaceous Pacific plate movement beneath SE China: Evidence from episodic volcanism and related intrusions: Tectonophysics, v. 614, p. 170–184, https://doi.org/10.1016/j.tecto.2013.12.007.

Liu, L., Xu, X.S., and Xia, Y., 2016, Asynchronizing paleo-Pacific slab rollback beneath SE China: Insights from the episodic Late Mesozoic volcanism: Gondwana Research, v. 37, p. 397–407, https://doi.org/10.1016/j.gr.2015.09.009.

Liu, L., Hu, R.Z., Zhong, H., Tang, Y.W., Yang, J.H., Li, Z., Zhao, J.L., and Shen, N.P., 2018, New constraints on the Cretaceous geodynamics of paleo-Pacific plate subduction: Insights from the Xiaojiang–Beizhang granitoids, Zhejiang Province, southeast China: Lithos, v. 314–315, p. 382–399, https://doi.org/10.1016/j.lithos.2018.06.020.

Liu, Q., Yu, J.H., Wang, Q., Su, B., Zhou, M.F., Xu, H., and Cui, X., 2012b, Ages and geochemistry of granites in the Pingtan–Dongshan Metamorphic Belt, Coastal South China: New constraints on Late Mesozoic magmatic evolution: Lithos, v. 150, p. 268–286, https://doi.org/10.1016/j.lithos.2012.06.031.

Liu, Y., Hu, Z., Zong, K., Gao, C., Gao, S., Xu, J., and Chen, H., 2010, Reappraisement and refinement of zircon U-Pb isotope and trace element analyses by LA-ICP-MS: Chinese Science Bulletin, v. 55, no. 15, p. 1535–1546, https://doi.org/10.1007/s11434-010-3052-4.

Ludwig, K.R., 2008, Manual for Isoplot 3.7: Berkeley Geochronology Center, Special Publication, v. 4, 77 p.

McDonough, W.F., and Sun, S.S., 1995, The composition of the Earth: Chemical Geology, v. 120, p. 223–253, https://doi.org/10.1016/0009-2541(94)00140-4.

McKay, M.P., Jackson, W.T., and Hessler, A.M., 2018, Tectonic stress regime recorded by zircon Th/U: Gondwana Research, v. 57, p. 1–9, https://doi.org/10.1016/j.gr.2018.01.004.

Meng, L., Li, Z.X., Chen, H., Li, X.-H., and Wang, X.C., 2012, Geochronological and geochemical results from Mesozoic basalts in southern South China Block support the flat-slab subduction model: Lithos, v. 132–133, p. 127–140, https://doi.org/10.1016/j.lithos.2011.11.022.

Miller, J.S., Matzel, J.E.P., Miller, C.F., Burgess, S.D., and Miller, R.B., 2007, Zircon growth and recycling during the assembly of large, composite arc plutons: Journal of Volcanology and Geothermal Research, v. 167, no. 1–4, p. 282–299, https://doi.org/10.1016/j.jvolgeores.2007.04.019.

Monani, S., and Valley, J.W., 2001, Oxygen isotope ratios of zircon: magma genesis of low $\delta^{18}O$ granites from the British Tertiary Igneous Province, western Scotland: Earth and Planetary Science Letters, v. 184, no. 2, p. 377–392, https://doi.org/10.1016/S0012-821X(00)00328-9.

Plank, T., Kelley, K.A., Zimmer, M.M., Hauri, E.H., and Wallace, P.J., 2013, Why do mafic arc magmas contain ~4 wt% water on average?: Earth and Planetary Science Letters, v. 364, p. 168–179, https://doi.org/10.1016/j.epsl.2012.11.044.

Qi, L., Hu, J., and Conrad, D., G., 2000, Determination of trace elements in granites by inductively coupled plasma mass spectrometry: Talanta, v. 51, no. 3, p. 507–513, https://doi.org/10.1016/S0039-9140(99)00318-5.

Richards, J.P., Spell, T., Rameh, E., Razique, A., and Fletcher, T., 2012, High Sr/Y magmas reflect arc maturity, high magmatic water content, and porphyry Cu ± Mo ± Au potential: Examples from the Tethyan arcs of central and eastern Iran and western Pakistan: Economic Geology and the Bulletin of the Society of Economic Geologists, v. 107, no. 2, p. 295–332, https://doi.org/10.2113/econgeo.107.2.295.

Rudnick, R.L., and Fountain, D.M., 1995, Nature and composition of the continental-crust: A lower crustal perspective: Reviews of Geophysics, v. 33, no. 3, p. 267–309, https://doi.org/10.1029/95RG01302.

Rudnick, R.L., and Gao, S., 2003, Composition of the continental crust, *in* Holland, H.D., and Turekian, K.K., eds., The Crust. Treatise on Geochemistry: Oxford, UK, Elsevier-Pergamon, https://doi.org/10.1016/B0-08-043751-6/03016-4, v. 3, p. 1–64.

Smythe, D.J., and Brenan, J.M., 2016, Magmatic oxygen fugacity estimated using zircon-melt partitioning of cerium: Earth and Planetary Science Letters, v. 453, p. 260–266, https://doi.org/10.1016/j.epsl.2016.08.013.

Spandler, C., and Pirard, C., 2013, Element recycling from subducting slabs to arc crust: A review: Lithos, v. 170–171, p. 208–223, https://doi.org/10.1016/j.lithos.2013.02.016.

Sun, W.D., Ding, X., Hu, Y.H., and Li, X.H., 2007, The golden transformation of the Cretaceous plate subduction in the west Pacific: Earth and Planetary Science Letters, v. 262, no. 3–4, p. 533–542, https://doi.org/10.1016/j.epsl.2007.08.021.

Tang, G.Q., Li, X.H., Li, Q.L., Liu, Y., Ling, X.X., and Yin, Q.Z., 2015, Deciphering the physical mechanism of the topography effect for oxygen isotope measurements using a Cameca IMS-1280 SIMS: Journal of Analytical Atomic Spectrometry, v. 30, no. 4, p. 950–956, https://doi.org/10.1039/C4JA00458B.

Tang, M., Wang, X.L., Shu, X.J., Wang, D., Yang, T., and Gopon, P., 2014, Hafnium isotopic heterogeneity in zircons from granitic rocks: Geochemical evaluation and modeling of "zircon effect" in crustal anatexis: Earth and Planetary Science Letters, v. 389, p. 188–199, https://doi.org/10.1016/j.epsl.2013.12.036.

Troch, J., Ellis, B.S., Harris, C., Ulmer, P., Bouvier, A.-S., and Bachmann, O., 2019, Experimental melting of hydrothermally altered rocks: Constraints for the generation of low-$\delta^{18}O$ rhyolites in the central Snake River Plain: Journal of Petrology, v. 60, no. 10, p. 1881–1902, https://doi.org/10.1093/petrology/egz056.

Valley, J.W., Kinny, P.D., Schulze, D.J., and Spicuzza, M.J., 1998, Zircon megacrysts from kimberlite: Oxygen isotope variability among mantle melts: Contributions to Mineralogy and Petrology, v. 133, no. 1–2, p. 1–11, https://doi.org/10.1007/s004100050432.

Valley, J.W., Lackey, J.S., Cavosie, A.J., Clechenko, C.C., Spicuzza, M.J., Basei, M.A.S., Bindeman, I.N., Ferreira, V.P., Sial, A.N., King, E.M., Peck, W.H., Sinha, A.K., and Wei, C.S., 2005, 4.4 billion years of crustal maturation: oxygen isotope ratios of magmatic zircon: Contributions to Mineralogy and Petrology, v. 150, no. 6, p. 561–580, https://doi.org/10.1007/s00410-005-0025-8.

Wang, D.Z., and Zhou, J.C., 2005, New progress in studying the Large Igneous Provinces [in Chinese with English abstract]: Gaoxiao Dizhi Xuebao, v. 11, no. 1, p. 1–8.

Wang, F.Y., Ling, M.X., Ding, X., Hu, Y.H., Zhou, J.B., Yang, X.Y., Liang, H.Y., Fan, W.M., and Sun, W., 2011a, Mesozoic large magmatic events and mineralization in SE China: Oblique subduction of the Pacific plate: International Geology Review, v. 53, no. 5–6, p. 704–726, https://doi.org/10.1080/00206814.2010.503736.

Wang, X.C., Li, Z.X., Li, X.H., Li, Q.L., Tang, G.Q., Zhang, Q.R., and Liu, Y., 2011b, Nonglacial origin for low-^{18}O Neoproterozoic magmas in the South China Block: Evidence from new in-situ oxygen isotope analyses using SIMS: Geology, v. 39, no. 8, p. 735–738, https://doi.org/10.1130/G31991.1.

Wang, Y.B., Zeng, Q.D., Zhang, S., Chen, P.W., and Gao, S., 2017, Spatial-temporal relationships of late Mesozoic granitoids in Zhejiang Province, Southeast China: Constraints on tectonic evolution: International Geology Review, v. 60, no. 11–14, p. 1529–1559, https://doi.org/10.1080/00206814.2017.1369176.

Wei, C.S., Zheng, Y.F., Zhao, Z.F., and Valley, J.W., 2002, Oxygen and neodymium isotope evidence for recycling of juvenile crust in northeast China: Geology, v. 30, no. 4, p. 375–378, https://doi.org/10.1130/0091-7613(2002)030<0375:OANIEF>2.0.CO;2.

Wiedenbeck, M., Hanchar, J.M., Peck, W.H., Sylvester, P., Valley, J., Whitehouse, M., Kronz, A., Morishita, Y., Nasdala, L., Fiebig, J., Franchi, I., Girard, J.P., Greenwood, R.C., Hinton, R., Kita, N., Mason, P.R.D., Norman, M., Ogasawara, M., Piccoli, P.M., Rhede, D., Satoh, H., Schulz-Dobrick, B., Skår, O., Spicuzza, M.J., Terada, K., Tindle, A., Togashi, S., Vennemann, T., Xie,

Q., and Zheng, Y.F., 2004, Further characterisation of the 91500 zircon crystal: Geostandards and Geoanalytical Research, v. 28, no. 1, p. 9–39, https://doi.org/10.1111/j.1751-908X.2004.tb01041.x.

Wong, Z.S., and Yu, F.M., 1999, Establishment of upper Cretaceous Xiaoxiong formation in coast of east Zhejiang [in Chinese]: Volcanology Mineral Resources, v. 20, no. 3, p. 197–204.

Wotzlaw, J.F., Bindeman, I.N., Schaltegger, U., Brooks, C.K., and Naslund, H.R., 2012, High-resolution insights into episodes of crystallization, hydrothermal alteration and remelting in the Skaergaard intrusive complex: Earth and Planetary Science Letters, v. 355–356, p. 199–212, https://doi.org/10.1016/j.epsl.2012.08.043.

Wu, F., Liu, X., Ji, W., Wang, J., and Yang, L., 2017, Highly fractionated granites: Recognition and research: Science China. Earth Sciences, v. 60, no. 7, p. 1201–1219, https://doi.org/10.1007/s11430-016-5139-1.

Xing, G.F., Yang, Z.L., Chen, R., Shen, J.L., Wei, N.Y., and Zhou, Y.Z., 2004, Three stages of Mesozoic bimodal igneous rocks and their tectonic implications on the continental margin of southeastern China: Acta Geologica Sinica-English Edition, v. 78, no. 1, p. 27–39.

Xu, X., O'Reilly, S.Y., Griffin, W.L., Wang, X., Pearson, N.J., and He, Z., 2007, The crust of Cathaysia: Age, assembly and reworking of two terranes: Precambrian Research, v. 158, no. 1–2, p. 51–78, https://doi.org/10.1016/j.precamres.2007.04.010.

Xu, X.S., O'Reilly, S.Y., Zhou, X.M., and Griffin, W.L., 1996, A xenolith-derived geotherm and the crust-mantle boundary at Qilin, southeastern China: Lithos, v. 38, no. 1–2, p. 41–62 https://doi.org/10.1016/0024-4937(95)00043-7.

Xu, X.S., Dong, C.W., Li, W.X., and Zhou, X.M., 1999, Late Mesozoic intrusive complexes in the coastal area of Fujian, SE China: The significance of the gabbro-diorite-granite association: Lithos, v. 46, no. 2, p. 299–315, https://doi.org/10.1016/S0024-4937(98)00087-5.

Xu, X.S., Zhao, K., He, Z.Y., Liu, L., and Hong, W.T., 2021, Cretaceous volcanic-plutonic magmatism in SE China and a genetic model: Lithos, v. 402–403, https://doi.org/10.1016/j.lithos.2020.105728.

Xue, S., Li, C., Qin, K., Yao, Z., and Ripley, E.M., 2018, Sub-arc mantle heterogeneity in oxygen isotopes: Evidence from Permian mafic-ultramafic intrusions in the Central Asian Orogenic Belt: Contributions to Mineralogy and Petrology, v. 173, no. 11, https://doi.org/10.1007/s00410-018-1521-y.

Yan, L.L., He, Z.Y., Beier, C., and Klemd, R., 2018, Geochemical constraints on the link between volcanism and plutonism at the Yunshan caldera complex, SE China: Contributions to Mineralogy and Petrology, v. 173, no. 1, https://doi.org/10.1007/s00410-017-1430-5.

Yang, Q., Xia, X., Zhang, W., Zhang, Y., Xiong, B., Xu, Y., Wang, Q., and Wei, G., 2018, An evaluation of precision and accuracy of SIMS oxygen isotope analysis: Solid Earth Sciences, v. 3, no. 3, p. 81–86, https://doi.org/10.1016/j.sesci.2018.05.001.

Yu, J.H., O'Reilly, S.Y., Wang, L., Griffin, W.L., Zhou, M.F., Zhang, M., and Shu, L., 2010, Components and episodic growth of Precambrian crust in the Cathaysia Block, South China: Evidence from U-Pb ages and Hf isotopes of zircons in Neoproterozoic sediments: Precambrian Research, v. 181, no. 1–4, p. 97–114, https://doi.org/10.1016/j.precamres.2010.05.016.

Zhang, J.H., Yang, J.H., Chen, J.Y., Wu, F.Y., and Wilde, S.A., 2018, Genesis of late Early Cretaceous high-silica rhyolites in eastern Zhejiang Province, southeast China: A crystal mush origin with mantle input: Lithos, v. 296–299, p. 482–495, https://doi.org/10.1016/j.lithos.2017.11.026.

Zhao, G., and Cawood, P.A., 2012, Precambrian geology of China: Precambrian Research, v. 222–223, p. 13–54, https://doi.org/10.1016/j.precamres.2012.09.017.

Zhao, J.H., Zhou, M.F., Yan, D.P., Zheng, J.P., and Li, J.W., 2011, Reappraisal of the ages of Neoproterozoic strata in South China: No connection with the Grenvillian orogeny: Geology, v. 39, no. 4, p. 299–302, https://doi.org/10.1130/G31701.1.

Zhao, J.H., Zhou, M.F., and Zheng, J.P., 2013, Constraints from zircon U-Pb ages, O and Hf isotopic compositions on the origin of Neoproterozoic peraluminous granitoids from the Jiangnan Fold Belt, South China: Contributions to Mineralogy and Petrology, v. 166, no. 5, p. 1505–1519, https://doi.org/10.1007/s00410-013-0940-z.

Zhao, J.H., Zhou, M.F., Wu, Y.B., Zheng, J.P., and Wang, W., 2019, Coupled evolution of Neoproterozoic arc mafic magmatism and mantle wedge in the western margin of the South China Craton: Contributions to Mineralogy and Petrology, v. 174, no. 4, https://doi.org/10.1007/s00410-019-1573-7.

Zheng, J.P., Griffin, W.L., Li, L.S., O'Reilly, S.Y., Pearson, N.J., Tang, H.Y., Liu, G.L., Zhao, J.H., Yu, C.M., and Su, Y.P., 2011, Highly evolved Archean basement beneath the western Cathaysia Block, South China: Geochimica et Cosmochimica Acta, v. 75, no. 1, p. 242–255, https://doi.org/10.1016/j.gca.2010.09.035.

Zhou, J.S., Yang, Z.S., Wang, Q., Zheng, Y.C., Hou, Z.-Q., and Wyman, D.A., 2020, Extraction of high-silica granites from an upper crustal magma reservoir: Insights from the Narusongduo magmatic system, Gangdese arc: The American Mineralogist, v. 105, no. 10, p. 1572–1584, https://doi.org/10.2138/am-2020-7369.

Zhou, X.M., and Li, W.X., 2000, Origin of Late Mesozoic igneous rocks in Southeastern China: Implications for lithosphere subduction and underplating of mafic magmas: Tectonophysics, v. 326, no. 3–4, p. 269–287, https://doi.org/10.1016/S0040-1951(00)00120-7.

Zhou, X.M., Sun, T., Shen, W.Z., Shu, L.S., and Niu, Y.L., 2006, Petrogenesis of Mesozoic granitoids and volcanic rocks in South China: A response to tectonic evolution: Episodes, v. 29, no. 1, p. 26–33, https://doi.org/10.18814/epiiugs/2006/v29i1/004.

Zhu, K.Y., Li, Z.X., Xu, X.S., Wilde, S.A., and Chen, H.L., 2016, Early Mesozoic ferroan (A-type) and magnesian granitoids in eastern South China: Tracing the influence of flat-slab subduction at the western Pacific margin: Lithos, v. 240–243, p. 371–381, https://doi.org/10.1016/j.lithos.2015.11.025.

Zou, H., Li, Q.L., Bagas, L., Wang, X.C., Chen, A.Q., and Li, X.H., 2021, A Neoproterozoic low-$\delta^{18}O$ magmatic ring around South China: Implications for configuration and breakup of Rodinia supercontinent: Earth and Planetary Science Letters, v. 575, https://doi.org/10.1016/j.epsl.2021.117196.

Science Editor: Wenjiao Xiao
Associate Editor: Laishi Zhao

Manuscript Received 1 January 2022
Revised Manuscript Received 7 May 2022
Manuscript Accepted 21 May 2022

Printed in the USA